

AperTO - Archivio Istituzionale Open Access dell'Università di Torino

**Influence of start-up phase of an incinerator on inorganic composition and lead isotope ratios of the atmospheric PM<sub>10</sub>**

**This is the author's manuscript**

*Original Citation:*

*Availability:*

This version is available <http://hdl.handle.net/2318/1783153> since 2021-04-15T22:33:43Z

*Published version:*

DOI:10.1016/j.chemosphere.2020.129091

*Terms of use:*

Open Access

Anyone can freely access the full text of works made available as "Open Access". Works made available under a Creative Commons license can be used according to the terms and conditions of said license. Use of all other works requires consent of the right holder (author or publisher) if not exempted from copyright protection by the applicable law.

(Article begins on next page)

1           **Influence of start-up phase of an incinerator on**  
2           **inorganic composition and lead isotope ratios of the**  
3           **atmospheric PM<sub>10</sub>**

4           Daniele Ziegler<sup>1</sup>, Mery Malandrino<sup>2\*</sup>, Claudia Barolo<sup>2</sup>, Gianpiero Adami<sup>3</sup>, Milena  
5           Sacco<sup>4</sup>, Francesco Pitasi<sup>4</sup>, Ornella Abollino<sup>5</sup>, Agnese Giacomino<sup>5</sup>

6           <sup>1</sup> Department of Applied Science and Technology, Polytechnic of Turin, Torino I-10129, Italy

7           <sup>2</sup> Department of Chemistry, NIS Interdepartmental and INSTM Reference Centre, University of Turin,  
8           Torino I-10125, Italy

9           <sup>3</sup> Department of Chemical and Pharmaceutical Sciences, University of Trieste, Trieste I-34127, Italy

10           <sup>4</sup> Piedmont Regional Agency for the Environmental Protection, Torino I-10135, Italy

11           <sup>5</sup> Department of Drug Science and Technology, University of Turin, University of Turin, Torino I-10125,  
12           Italy

13  
14           Corresponding author. Mery Malandrino Via P. Giuria 5, 10125 Torino Italy.

15           E-mail address: mery.malandrino@unito.it (M. Malandrino).

16

17 **Abstract:**

18 A municipal solid waste incinerator (MSWI) was installed in a peripheral area of the city of Turin. In this  
19 study, we evaluated the contribution of this plant to the massive concentration of PM<sub>10</sub>, to its chemical  
20 composition and to the distribution of the lead isotopes during the start-up phase.

21 We assessed the inorganic composition of PM<sub>10</sub> collected in the vicinity of the Turin incinerator by  
22 inductively coupled plasma atomic emission spectroscopy (ICP-AES), magnetic sector inductively coupled  
23 plasma mass spectrometer (SF-ICP-MS) and ion chromatography (IC). The lead isotope ratios in PM<sub>10</sub>  
24 samples were determined by SF-ICP-MS by a method developed and optimized using experimental design  
25 approach.

26 Element trends and data chemometric treatment evidence that the vehicular traffic, increased in this area  
27 due to the opening of the MSWI plant, and, to a lesser degree, the direct incinerator emissions influence  
28 As, Cd, Cr, Cu, Ba, Mo, Pb, Sn and Zn concentrations. As a whole, however, the element concentrations in  
29 PM<sub>10</sub> and the Enrichment Factors (EFs) were comparable with the values reported for other urban sites and  
30 target pollutant concentrations of MSWI emissions, namely Cd, Cr, Cu and Pb, were lower than in PM<sub>10</sub>  
31 emitted from older MSWIs. This confirms that incinerators of new installation have a lower impact on  
32 atmospheric PM<sub>10</sub> composition thanks to stricter current legislation and up-to-date technologies. The lead  
33 isotope ratios investigation allowed to distinguish the diverse sources (crustal, vehicular traffic and MSWI)  
34 that influence lead concentration in PM<sub>10</sub> collected near incinerator during start-up phase.

35

36 **Keywords:**

37

38 Incinerator; Trace elements in PM<sub>10</sub>; Chemometric processing; Lead isotope ratios

39

40 **List of Abbreviations**

41 MSWI           Municipal Solid Waste Incinerator

42	IC	Ion Chromatography
43	ICP-AES	Inductively Coupled Plasma Atomic Emission Spectroscopy
44	SF-ICP-MS	Magnetic Sector Inductively Coupled Plasma Mass Spectrometer
45	EFs	Enrichment Factors
46	PM	Particulate Matter
47	WSI	Water Soluble Ions
48	TRM	Trattamento di Rifiuti Metropolitani
49	PCA	Principal Component Analysis
50	HCA	Hierarchical Cluster Analysis
51	CCD	Central Composite Design
52	PLS	Partial Least Square
53	PBL	Planetary Boundary Layer

54

## 55 **1. Introduction**

56 Air pollution represents one of the greatest concerns of urban environments. During the last decades great  
57 attention was paid to Particulate Matter (PM), due to the correlation between fine PM exposure and adverse  
58 health effects. The damage to health correlated to PM air pollution is one of the main environmental issues  
59 raised by World Health Organization.

60 The Po Valley covers the territory of several regions in Northern Italy and includes many urban  
61 agglomerates, such as Turin, Milan, Venice and Bologna. The area is densely populated and heavily  
62 industrialized. High amounts of atmospheric pollutants, e.g. about 400.000 tons of NO<sub>x</sub>, 80.000 tons of PM  
63 and 250.000 tons of NH<sub>3</sub> (ammonia), are emitted per year by a wide variety of pollution sources, which are  
64 mainly related to traffic, domestic heating, industry and energy production, agriculture and farming  
65 activities (Raffaelli et al., 2020). Furthermore, the geographic conformation prevents an efficient dispersion  
66 of primary pollutants and causes a consequent high formation of secondary pollutants. The European

67 Environmental Agency indicated the Po Valley as a hot spot region for air pollutants, in particular for NO<sub>2</sub>  
68 in 2013 (EEA, 2013 and 2015).

69 The mechanisms responsible for the biological effects of particulate matter have been continuously  
70 undergone review, and many questions are still open about some relevant aspects, for example size fraction,  
71 number or mass of the particles, chemical components, among which metal elements are relevant species.  
72 Metals generally occur as different chemical compounds and in different oxidation states and are distributed  
73 among various dimensional fractions of the PM in the troposphere. Transport and distribution of aerosol  
74 particles strictly depend on their size, as well as to the weather conditions (Poschl, 2005).

75 Concentration, composition and size distribution of atmospheric particles are temporally and spatially  
76 highly variable. Altogether, however, particles size depends primarily on emission sources, and typically  
77 those emitted from anthropogenic sources are smaller than those emitted from natural ones (Harrison et al.,  
78 2012).

79 On the base of existing scientific evidence, many metals (often depending on their oxidation state) may  
80 have a direct or indirect active role in PM biological mechanisms of action.

81 Municipal solid waste incinerators (MSWIs) can be significant sources of atmospheric environmental  
82 pollution, potentially exposing nearby populations to hazardous chemicals at toxic levels. Both inorganic  
83 and organic chemicals have been identified in MSWI emissions, for instance carbon monoxide (CO), carbon  
84 dioxide (CO<sub>2</sub>), sulphur oxides (SO<sub>x</sub>), nitrogen oxides (NO<sub>x</sub>), dioxins and furans, volatile organic  
85 compounds (VOC), polycyclic aromatic hydrocarbons (PAHs), metals and particulate matter (PM) (WHO,  
86 2007). Some of these chemicals have been classified as known (group 1) or probable (group 2A)  
87 carcinogens for humans according to the International Agency for Research on Cancer (IARC, 2012). Some  
88 studies have suggested associations between MSWI emissions and health effects, particularly adverse  
89 impacts on reproduction and cancer (Vinceti et al., 2008).

90 Because of these troubles that have been identified in earlier studies, more recent investigations have been  
91 designed and implemented with the goal of establishing a better definition of exposure and/or effects arising  
92 from MSWIs.

93 Directive 2000/76/EC of the European Parliament and the Council on Incineration of Waste enforces  
94 measures to prevent or reduce negative effects to the environment, particularly emissions into air, soil and  
95 surface water, as well as to human health, which might arise from incineration and co-incineration of waste.  
96 More in detail, this directive states that incineration facilities shall be submitted to a permission to operate,  
97 which sets rigorous operating conditions, technical requirements and daily emission limits of  $10 \text{ mg/m}^3$  for  
98 total dust and  $0.5 \text{ mg/m}^3$  for the sum of Sb, As, Pb, Cr, Co, Cu, Mn, Ni and V (Directive 2000/76/EC, 2010).  
99 When discussing the environmental characteristics of a specific region, the identification of various sources  
100 of a pollutant becomes significant; consequently, the MSWI presence must be considered as a possible  
101 source of pollutants in airborne particulate matter. The knowledge of the metal content in PM is also  
102 important in recognizing its sources since these emit airborne PM with different metal distribution. MSWIs,  
103 indeed, play an important role in the treatment of municipal waste according to the recent European  
104 directives and it is very important to know the contribution of a MSWI plant of new generation to the  
105 inorganic composition of atmospheric  $\text{PM}_{10}$ . Many studies have evaluated the impact of MSWIs on air  
106 quality (Carignan et al., 2005; Pacyna et al., 2007; Font et al., 2015; Panepinto et al., 2018; Lucarelli et al.,  
107 2019) but, to our knowledge, none of these has evaluated the contribution during start-up phase.

108 Pb is a poisonous metal that can damage nervous connections especially in young children and cause blood  
109 and brain disorders (Tong et al., 2000; Gerhardsson, 2004; Meyer et al., 2008). The concentration of this  
110 heavy metal in PM is regulated by the Directive 2008/50/EC, which establishes a limit value of  $0.5 \text{ }\mu\text{g/m}^3$   
111 for a calendar year (Directive 2008/50/EC, 2008). Although lead occurs naturally in the environment, most  
112 of the high levels found throughout the environment derived from human activities. The European Union  
113 established the 1<sup>st</sup> of January 2000, as a limit date to remove leaded fuel from the market, although the  
114 European Commission conceded derogation to Spain, Italy and Greece until the 1<sup>st</sup> of January 2002. That  
115 is the reason why the concentration of this element in air has been decreasing since then, although other  
116 anthropogenic sources persist, such as smelting, steel mills, incineration of residues, wood and coal  
117 combustion, resuspension of contaminated soil dust and industrial activities (production of paintings,  
118 chemical agents, welds, etc.) (Widory et al., 2004, 2010; Zhao et al., 2017, 2019; Xu et al., 2020). The

119 identification of stable lead isotope composition in atmospheric particulate matter of several cities around  
120 the world is being increasingly used to better characterize atmospheric lead sources (Carignan et al., 2005;  
121 Komarek et al., 2008; Guéguen et al., 2012; Gioia et al., 2010, 2017; Zhao et al. 2019; Lee et al., 2019; Xu  
122 et al., 2020).

123 This study focuses on:

- 124 • evaluation of the contribution of a new MSWI plant in start-up phase to total  $PM_{10}$  and its chemical  
125 composition in water soluble ions (WSI) and major, minor and trace elements;
- 126 • development, thorough an Experimental Design approach, of an accurate method for the calculation  
127 of lead isotope ratios using microwave acid digestion followed by magnetic sector inductively  
128 coupled plasma mass spectrometer (SF-ICP-MS) determination;
- 129 • discrimination between different sources of lead, known to be a marker of incinerator's emission,  
130 through a study of its isotope ratios.

131

## 132 **2. Materials and methods**

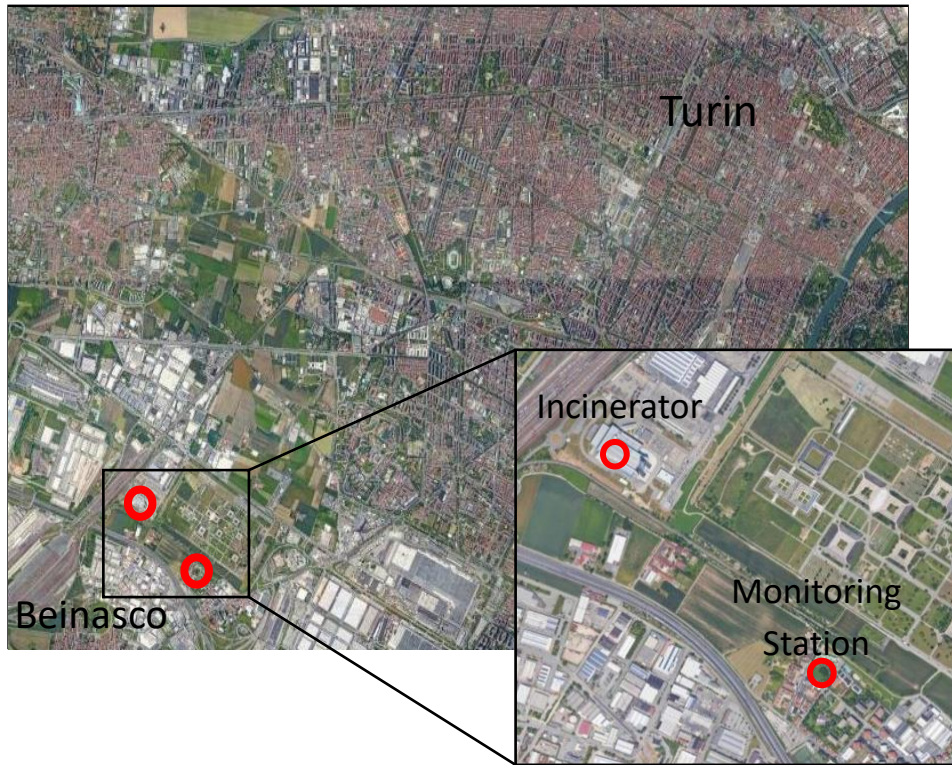
### 133 ***2.1 Sampling location and $PM_{10}$ collection***

134 An incinerator was built in the city of Turin, a metropolitan area characterized by many industrial activities  
135 and huge volume of vehicular traffic, between 2010 and 2013 and initially was authorized to receive a  
136 maximum of 421,000 tons of waste per year from the province of Turin and from other regions. In July  
137 2015, following revision of the Integrated Environmental Authorization, the plant's capacity was stepped  
138 up to 490,000 tons per year. This plant is precisely located in the south-western zone of Turin outskirts. It  
139 converts municipal solid waste, as well as special waste that can be combined with the municipal waste (up  
140 to a maximum of 124,000 tons per year), into electrical and thermal energy. More in detail, it consists in a  
141 moving grate with four methane burners able to produce 41 MW of electrical power and 106 MW of district  
142 heating simultaneously. It is managed by a metropolitan waste treatment society (Trattamento di Rifiuti

143 Metropolitani – TRM S.p.A.); for this reason, the sampling location is hereinafter referred to as TRM  
144 (<http://trm.to.it/>).

145 PM<sub>10</sub> sampling was carried out in spring and summer 2013 in one site localized near the incinerator, in the  
146 area with the highest probability that PM emitted from the plant is falling to the ground. Air quality  
147 monitoring station is placed at 45°02'45" N and 7°37'00" E, in the Aldo Mei park of Beinasco town  
148 (Province of Turin) and it is managed by Regional Agency for Environmental Protection (ARPA,  
149 Piedmont). It is equipped with several instruments (PM<sub>10</sub> and PM<sub>2.5</sub> Beta Attenuation Mass Monitor, Swam  
150 5A Dual Channel model, FAI instruments; Analyzer for Nitrogen Compounds, 200E model, Teledyne API;  
151 PM<sub>10</sub> Sampler, with a Sentinel 96 module for the automatic sequential sampling, Charlie model, TCR  
152 Tecora; dioxins/furans Sampler, ECHO HiVol model, TCR Tecora; Wet&Dry Deposimeter Samplers for  
153 dioxins/furans and polycyclic aromatic hydrocarbons, Labservice Analytica; Air Mercury Monitor, RA-  
154 915 AM model, Lumex) to detect specific air pollutants like NO<sub>x</sub>, gaseous Hg, PM<sub>10</sub> and PM<sub>2.5</sub> mass  
155 concentrations. A map of the metropolitan area, showing the position of the incinerator and the monitoring  
156 station, is reported in Figure 1.





158 *Figure 1: Geographical map of Piedmont and detail of the position of the incinerator and the monitoring*  
159 *station.*

160  
161 The PM<sub>10</sub> samples were collected using a high-volume air sampler (Digitel DHA) and 80 and 150 mm  
162 diameter quartz filters to ensure a large amount of PM<sub>10</sub> that would allow also the lead isotopic  
163 investigation. Sampling duration for each sample was fixed at 24 hours, at a flow of 29 m<sup>3</sup>/h for a total  
164 volume of sampled air of 700 m<sup>3</sup>.

165 A low volume air sampler, at a flow rate of 2.3 m<sup>3</sup>/h and equipped with 47 mm diameter quartz filter, was  
166 adopted in order to evaluate daily mass concentration of PM<sub>10</sub>. The flow control was carried out in the  
167 actual condition mode and the mass concentrations of PM<sub>10</sub> were measured by weighing each filter before  
168 and after sampling on an analytical balance in a controlled atmosphere (20 °C, 50% relative humidity)  
169 according to Ministerial Decree 60/2002 (D.Lgs. 60, 2002). Meteorological conditions (i.e. average and  
170 maximum wind speed, average and maximum mixing height, and average temperature) were obtained from  
171 the Minerve calculation model, a diagnostic model for the reconstruction of three-dimensional wind and  
172 temperature fields (Table 1S Supplementary Material).

173

## 174 ***2.2 Choice of PM10 samples***

175 The activity of Turin MSWI plant started on 19th April 2013, by testing the first combustion line. Then,  
176 from 22 May to 5 June also the second combustion line began to be active. Subsequently, from 5 June, the  
177 second combustion line of the plant was suspended, and it started again the activity in July.

178 Twenty-two samples were chosen for this study in the period between May and July 2013. The choice was  
179 performed considering the most representative days, based on the evaluation of two statistical methods:  
180 Principal Component Analysis (PCA) and Hierarchical Clustering Analysis (HCA) (shown in figure 1S, 2S  
181 and 3S in Supplementary Material).

182 Both meteorological parameters, obtained by a weather station located in the site, such as average and  
183 maximum wind speed (m/s), average temperature, average and maximum mixing height, and chemical

184 parameters, such as  $PM_{10}$ ,  $PM_{2.5}$ ,  $NO_2$  and  $NO$  concentrations (Table 1S), were considered, obtaining a  
185 dataset composed by 56 samples and 9 variables. These data were supplied by ARPA Piedmont.  
186 All chemometric elaborations were carried out after autoscaling of the data. PC1 and PC2 collect the 62.6%  
187 (41.6% and 21% respectively) of total variance.  
188 More in detail, from loading plot it was clear that both  $PM_{10}$  and  $PM_{2.5}$  amounts are anticorrelated with  
189 wind speed, as expected; as a matter of fact, the samples collected in May are characterized by negative  
190 scores values on PC1, suggesting that these samples are most influenced by wind speed variable. This is  
191 true especially for samples 25 and 26 May (25/5 and 26/5), two weekend days, when the airborne particulate  
192 emitted by tracks is consistently reduced; these samples, together with 29 May (29/5) and 31 May (31/5),  
193 show the minimum amount of  $PM_{10}$  and, in the score plot, are placed in opposite position to the vector  
194 representing this variable.  
195 In fact, during May, higher speed of wind values was recorded, resulting in an enhanced dispersion of  
196 particulate matter respect to the summer period. Surprisingly, temperature variable is quite correlated to  
197  $PM_{10}$  amount in troposphere. This phenomenon can be due to the enhanced rainfall recorded in May,  
198 resulting in a decrease of both temperature and coarse fraction of particulate matter. Moreover,  $NO$   
199 concentration appears anti-correlated with mixing height.  $NO$  presence has an influence in the concentration  
200 of  $NO_2$ , that is obtained from the former after a photochemical oxidation in troposphere due to ozone. In  
201 the month of May,  $NO$  concentration is higher than in June and July, due to the lower height of the PBL  
202 (Planetary Boundary Layer). Finally,  $PM_{10}$  and  $PM_{2.5}$  concentrations are correlated with  $NO_2$  concentration,  
203 and they are also anti-correlated with the wind speed as seen in Yadav et al. (2014), describing a more  
204 polluted environment for higher  $PM$  and  $NO_2$  concentrations. This phenomenon is verified especially for  
205 three weekdays, 17, 18 and 19 June (17/6, 18/6 and 19/6), in which samples are characterized by  $PM_{10}$   
206 concentrations up to  $30 \mu\text{g}/\text{m}^3$  with a reduced transport of particulate matter over long distances.  
207 In addition, through HCA three main clusters were detected: a cluster composed by the samples collected  
208 at the end of May, displaying lower  $PM_{10}$  concentrations and other two clusters comprising the samples  
209 from June and July separated according to  $PM_{10}$  concentrations and the weather conditions.

210 We chose PM<sub>10</sub> samples considering the results obtained from both chemometric techniques: PM<sub>10</sub> samples  
211 more influenced by PC1 and PC2 and representing evenly the clusters evidenced by HCA were selected.  
212 PM<sub>10</sub> samples having the highest and the lowest PM<sub>10</sub> concentration in each month were also selected. Our  
213 selection criterion has permitted us to compare days with a high and a low concentration of particulate  
214 matter and to provide information on the dominant sources of atmospheric aerosol in the investigated area,  
215 even if we cannot consider this selection as representative of the possible patterns of atmospheric pollutants  
216 in the whole period.

217

## 218 ***2.2 Element and WSI determination***

219 All filters have been analyzed to determine the mass of particulate collected using a gravimetric technique  
220 according to Ministerial Decree 155/ 2010 (D.Lgs. 155, 2010).

221 The aerosol-loaded filters (143 mm of the total 150 mm diameter) were punched into 36 mm diameter  
222 circular sections. The determination of elements and WSI was executed in duplicate and, for each replicate,  
223 two aliquots of each filter were considered. This approach showed that PM<sub>10</sub> distribution on filters was  
224 equable. In fact, relative standard deviation (RSD) was <10% for all the elements except for potassium with  
225 a value equal to 15%.

226 Each sub-sample for element determination was digested by a microwave oven (Milestone-Ethos One) with  
227 a mixture of 3.5 mL of sub-boiled HNO<sub>3</sub>, 1.5 mL of ultra-pure H<sub>2</sub>O<sub>2</sub> (Sigma-Aldrich) and 3 mL of HPW  
228 (Milli-Q (Millipore) ultrapure water, resistivity = 18.2 MΩ cm) in 100 mL tetrafluoromethoxyl vessels. The  
229 following heating steps were applied: 5 min ramp until 170 °C, 10 min dwell at 170 °C, 5 min ramp until  
230 200 °C, 20 min dwell at 200 °C, and 30 min of ventilation. The resulting solutions were filtered on cellulose  
231 filters (Whatman Grade 5) to eliminate the undissolved filter parts and diluted to 30 mL with HPW. By this  
232 method, the concentrations of trace elements not enclosed in silicate matrix were transferred quantitatively  
233 into solution.

234 Elements present in lower concentrations were determined by SF-ICP-MS (Thermo Finnigan Element 2).

235 Mass resolution and isotope selection were optimized for each element to ensure resolution of spectral

236 interferences and maximize sensitivity. The following isotopes of the investigated elements were  
237 monitored:  $^{47}\text{Ti}$ ,  $^{48}\text{Ti}$ ,  $^{51}\text{V}$ ,  $^{53}\text{Cr}$ ,  $^{63}\text{Cu}$ ,  $^{65}\text{Cu}$ ,  $^{68}\text{Zn}$ ,  $^{75}\text{As}$ ,  $^{90}\text{Zr}$ ,  $^{95}\text{Mo}$ ,  $^{98}\text{Mo}$ ,  $^{111}\text{Cd}$ ,  $^{112}\text{Cd}$ ,  $^{114}\text{Cd}$ ,  $^{118}\text{Sn}$ ,  $^{138}\text{Ba}$ ,  
238  $^{207}\text{Pb}$ ,  $^{208}\text{Pb}$  at low resolution ( $R=400$ );  $^{46}\text{Ti}$ ,  $^{59}\text{Co}$ ,  $^{60}\text{Ni}$ ,  $^{61}\text{Ni}$ ,  $^{62}\text{Ni}$ ,  $^{64}\text{Zn}$ ,  $^{66}\text{Zn}$ ,  $^{96}\text{Mo}$ ,  $^{113}\text{Cd}$ ,  $^{139}\text{La}$ ,  $^{140}\text{Ce}$ ,  $^{203}\text{Tl}$ ,  
239  $^{205}\text{Tl}$ ,  $^{204}\text{Pb}$ ,  $^{206}\text{Pb}$  at medium resolution ( $R=4,000$ ). Analyses on each sample were conducted following a  
240 60s uptake and stabilization period. In low resolution 9 replications (3 run x 3 passes) for each selected  
241 isotope were carried out, while in medium resolution 12 replications (4 run x 3 passes) for every isotope  
242 were carried out. Between samples the nebulizer system was rinsed for 2 min with 2% sub-boiled  $\text{HNO}_3$ ,  
243 which eliminated carry-over and reconditioned the sampler cone. Power applied was 1270 W, 1 L/min flow  
244 of both auxiliary and nebulizer gasses, while plasma gas was fluxed at 16 L/min.

245 The following elements: Ca, Al, Na, K, Mg, Mn and Fe present in higher concentrations in PM samples,  
246 were determined by Inductively Coupled Plasma Atomic Emission Spectroscopy, ICP-AES (Perkin Elmer,  
247 model Optima 7000 DV).

248 The power applied was 1300 W. Plasma, auxiliary and nebulizer gas flows were 15, 0.2 and 0.6 L/min  
249 respectively. The signals were measured in triplicate.

250 Sets of instrumental blank and calibration verification checks were run at frequent intervals during the batch  
251 sequences for both SF-ICP-MS and ICP-AES analyses. The calibrations were performed with standard  
252 solutions prepared in aliquots of process blanks. Process blanks were incorporated into the dissolution and  
253 analytical procedure to assess metal contribution from the filters, bombs, Milli-Q water and purified acids  
254 used in this procedure. Limits of detection (LODs), corresponding to three times the standard deviation of  
255 the reagent blank, were experimentally determined by ICP-AES and SF-ICP-MS and are respectively  
256 reported in Table 2S and 3S (Supplementary Material).

257 All the elements investigated, namely Al, As, Ba, Ca, Cd, Ce, Co, Cr, Cu, Fe, K, La, Mg, Mn, Mo, Na, Ni,  
258 Pb, Sn, Ti, Tl, V, Zn and Zr, are commonly used, with the aid of chemometric treatments and other graphical  
259 and mathematical tools, as chemical markers for identifying the anthropogenic and natural (crustal and  
260 marine) sources of atmospheric PM.

261 Sampling was carried out over three months, namely May-July 2013, using two distinct types of filters:  
262 Millipore© for the first month and Munktell for the remaining time. The sample blank values were  
263 measured for each filter type and all the sample signals were subtracted of their appropriate sample blank  
264 values. Sample blank concentrations ( $\mu\text{g/L}$  or  $\text{ng/L}$ ) are reported in Table 2S and 3S.  
265 NIST SRM 1648a (Urban Particulate Matter) and NIES CRM 8 (Vehicle Exhaust Particulates) were used  
266 for evaluating the procedural recoveries and for identifying the best analytical parameters. Most of the  
267 relative errors for the analytes are lower than 10%, except for some elements of geogenic origin like Al,  
268 La, Ce and Ti, which are unlikely to be completely extracted without HF.  
269 Finally, the WSI concentrations were determined using an Ion Chromatography (IC) system (Dionex, DX-  
270 100, configuration DX 500 for anions and configuration DX 320 for cations). Four circular filter sections  
271 (36 mm diameter) for two replicates were placed in 10 mL of HPW and sonicated for 30 minutes to obtain  
272 an extraction solution, which was then filtered using a 0.22  $\mu\text{m}$  pore syringe filter. The anion ( $\text{NO}_3^-$ ,  $\text{Cl}^-$  and  
273  $\text{SO}_4^{2-}$ ) concentrations were measured using an AS11-HC column (4 x 250 mm) with 30 mM KOH while  
274 the cation ( $\text{NH}_4^+$ ,  $\text{Na}^+$ ,  $\text{K}^+$ ,  $\text{Mg}^{2+}$  and  $\text{Ca}^{2+}$ ) concentrations were determined using an Ion Pac CS12A column  
275 (4 x 250 mm) with 20 mM methanesulfonic acid as an eluent at a flow rate of 1.0 mL/min. LOD and sample  
276 blank concentrations for WSI are reported in Table 4S (Supplementary Material).

277

### 278 ***2.3 Statistic Data Analysis***

279 The chemometric treatment was carried out using XlStat 2017 software package, an add-on of Microsoft  
280 Excel. PCA is a statistical method that uses an orthogonal conversion of a group of observations of possibly  
281 correlated variables into a set of uncorrelated variables, obtained by linear combination of the original ones,  
282 called principal components (PCs). The number of PCs is less than or equal to the number of original  
283 variables. The first principal component has the largest possible variance and the resulting vectors are an  
284 uncorrelated orthogonal basis set (Cohen et al., 2003). HCA is a method of group analysis which explores  
285 the dataset to build a hierarchy of clusters. An agglomerative procedure was used for clustering: this is a  
286 "bottom up" approach, in which each observation starts in its own cluster, and pairs of clusters are merged

287 as one moves up the hierarchy (Rokach and Maimon, 2005). For performing PCA and HCA, the whole  
288 dataset was autoscaled. Finally, Kruskal-Wallis test (significance level: 95% and 90%) was performed for  
289 checking if the analyte concentrations determined in PM<sub>10</sub> samples collected in 2012, 2013 and 2014 in  
290 TRM monitoring station were significantly different. The same non-parametric test was used to evaluate if  
291 As, Cd, Ni and Pb concentrations in PM<sub>10</sub> samples collected in Druento, Torino-Consolata and TRM  
292 monitoring stations in 2013 and in May, June and July months in 2014-2018 years were significantly  
293 different.

294

### 295 ***2.3 SRM-Lead isotope ratios analysis***

296 The evaluation of lead isotopic ratios was carried out by SF-ICP-MS considering two circular filter sections  
297 of 36 mm of diameter. These sections were punched using an INOX punch: in this way, an enhanced  
298 accuracy is guaranteed compared to dividing the filter in four parts using clippers. In fact, the relative  
299 standard deviations of replicates were always lower than 10%.

300 In order to evaluate lead isotope ratios, a NIST SRM 981 (Common lead isotopic standard) was used. This  
301 certified standard reflects the natural abundance of four lead isotopes: 204 ( $1.4255 \pm 0.0012\%$ ), 206  
302 ( $24.1442 \pm 0.0057\%$ ), 207 ( $22.0833 \pm 0.0027\%$ ), 208 ( $52.347 \pm 0.0086\%$ ).

303 SRM 981 was utilized for correcting the bias introduced by instrumental mass discrimination. A solution  
304 containing 1.2 mg/L of lead in 0.05% ultrapure nitric acid matrix was prepared for that objective. The values  
305 used for the mass bias correction were  $0.059042 \pm 0.000037$ ,  $0.91464 \pm 0.00033$ ,  $2.1681 \pm 0.0008$   
306 respectively for 204/206, 207/206 and 208/206 ratio, as reported on the certificate released by NIST, with  
307 errors calculated at 95% confidence interval.

308 A Central Composite Design (CCD) with a total of 27 experiments was chosen to optimize the following  
309 instrumental parameters was carried out:

- 310 • Integration window (window of masses to integrate peaks)
- 311 • Sampling points per peak (number of points counted in the window of masses chosen)

312       • Integration times (runs x passes), equal to the replications.  
313 The ranges used for these parameters were 60-100%, 5-30 and from 1x1 to 9x9 respectively. These ranges  
314 were applied also by Zhu et al. (2006).  
315 After evaluating lead concentration in samples analyzed, the concentrations of 2.5 µg/L and 25 µg/L of lead  
316 in SRM 981 were chosen, respectively equal to the minimum and the maximum Pb concentration in the  
317 samples. In addition, all the measurements were carried out working in both low and medium resolution.  
318 In this work, the number of factors ( $k$ ) is equal to 4 (integration window, sampling points per peak, runs  
319 and passes) and 2 levels ( $L$ ) for each factor were assigned (minimum and maximum value of above reported  
320 ranges). Experiments to be realized are equal to  $L^k + L * k + n$ , where  $n$  is the number of the central points  
321 (three in this case) (Lundstedt et al., 1998). This chemometric approach was carried out within the software  
322 Modde 9.1 (<https://umetrics.com/product/modde>).

323

## 324 **3. Results and discussion**

### 325 ***3.1 Chemical composition***

#### 326 ***3.1.1 Mass and element concentrations***

327 The PM<sub>10</sub> and element concentrations (mean, standard deviation, and 5th - 95th percentiles) for each month  
328 (May, June and July) are reported in Table 1 while PM<sub>10</sub> and element concentrations (mean and standard  
329 deviation) in each PM<sub>10</sub> sample are shown in Tables 5S, 6S and 7S (Supplementary Material).

330



331 **Table 1.** Mean and standard deviation (Mean  $\pm$  SD), and 5<sup>th</sup> - 95<sup>th</sup> percentiles of each element determined in PM<sub>10</sub>  
 332 samples and PM<sub>10</sub> massive concentration, divided by month. All values, except for PM<sub>10</sub>, are expressed in ng/m<sup>3</sup>. PM<sub>10</sub>  
 333 is expressed in  $\mu\text{g}/\text{m}^3$ .

Element	May		June		July	
	Mean $\pm$ SD	5 <sup>th</sup> - 95 <sup>th</sup> perc.	Mean $\pm$ SD	5 <sup>th</sup> - 95 <sup>th</sup> perc.	Mean $\pm$ SD	5 <sup>th</sup> - 95 <sup>th</sup> perc.
<b>PM<sub>10</sub></b>	9 $\pm$ 5	5 - 17	31 $\pm$ 4	24 - 35	23 $\pm$ 3	20 - 27
<b>Al</b>	155 $\pm$ 63	90 - 228	477 $\pm$ 205	207 - 688	326 $\pm$ 137	171 - 522
<b>As</b>	0.61 $\pm$ 0.05	0.55 - 0.68	0.80 $\pm$ 0.31	0.46 - 1.23	0.41 $\pm$ 0.09	0.30 - 0.54
<b>Ba</b>	6.05 $\pm$ 1.34	4.50 - 7.93	30.0 $\pm$ 25.0	7.05 - 61.6	35.1 $\pm$ 16.7	12.9 - 49.9
<b>Ca</b>	235 $\pm$ 96	140 - 350	575 $\pm$ 208	296 - 808	354 $\pm$ 139	186 - 530
<b>Cd</b>	0.05 $\pm$ 0.04	0.03 - 0.11	0.08 $\pm$ 0.02	0.06 - 0.11	0.08 $\pm$ 0.01	0.06 - 0.09
<b>Ce</b>	0.16 $\pm$ 0.07	0.08 - 0.25	0.46 $\pm$ 0.23	0.14 - 0.73	0.21 $\pm$ 0.15	0.08 - 0.42
<b>Co</b>	0.08 $\pm$ 0.06	0.03 - 0.16	0.28 $\pm$ 0.35	0.06 - 0.81	0.10 $\pm$ 0.04	0.05 - 0.15
<b>Cr</b>	0.67 $\pm$ 0.57	0.07 - 1.26	3.83 $\pm$ 2.43	0.64 - 6.63	3.29 $\pm$ 1.19	1.63 - 4.63
<b>Cu</b>	9.39 $\pm$ 1.58	7.37 - 11.4	18.6 $\pm$ 3.80	12.8 - 22.4	14.3 $\pm$ 3.83	9.73 - 19.8
<b>Fe</b>	288 $\pm$ 66	210 $\pm$ 365	631 $\pm$ 207	347 - 848	440 $\pm$ 161	251 - 675
<b>K</b>	81.9 $\pm$ 39.3	39 - 133	251 $\pm$ 69	157 - 318	187 $\pm$ 52	140 - 266
<b>La</b>	0.10 $\pm$ 0.04	0.06 - 0.16	0.35 $\pm$ 0.15	0.14 - 0.53	0.21 $\pm$ 0.10	0.11 - 0.37
<b>Mg</b>	142 $\pm$ 80	75 - 254	307 $\pm$ 128	137 - 445	204 $\pm$ 89	101 - 328
<b>Mn</b>	6.30 $\pm$ 1.26	5.33 - 8.25	24.4 $\pm$ 8.7	12.6 - 33.8	14.3 $\pm$ 5.4	8.51 - 21.1
<b>Mo</b>	0.32 $\pm$ 0.11	0.19 - 0.46	0.82 $\pm$ 0.19	0.55 - 1.02	0.67 $\pm$ 0.17	0.45 - 0.89
<b>Na</b>	302 $\pm$ 365	18 - 775	137 $\pm$ 28	96 - 165	76.6 $\pm$ 34	35 - 117
<b>Ni</b>	1.56 $\pm$ 0.66	0.89 - 2.45	3.86 $\pm$ 0.92	2.63 - 4.89	2.37 $\pm$ 0.74	1.59 - 3.48
<b>Pb</b>	1.17 $\pm$ 0.63	0.60 - 2.11	4.81 $\pm$ 1.58	2.88 - 6.98	3.16 $\pm$ 0.74	2.30 - 4.15
<b>Sn</b>	2.91 $\pm$ 0.80	1.77 - 3.73	5.38 $\pm$ 0.91	4.20 - 6.43	3.96 $\pm$ 0.90	2.79 - 5.20
<b>Ti</b>	5.29 $\pm$ 1.65	3.54 - 7.17	14.5 $\pm$ 6.55	6.13 - 21.7	10.7 $\pm$ 4.10	5.96 - 16.4
<b>Tl</b>	0.004 $\pm$ 0.002	0.002 - 0.007	0.019 $\pm$ 0.005	0.013 - 0.025	0.013 $\pm$ 0.002	0.010 - 0.015
<b>V</b>	0.85 $\pm$ 0.81	0.24 - 2.10	3.14 $\pm$ 0.93	2.04 - 4.24	1.17 $\pm$ 0.37	0.71 - 1.62
<b>Zn</b>	14.5 $\pm$ 5.2	8.60 - 21.3	29.3 $\pm$ 13.5	13.0 - 47.0	24.5 $\pm$ 11.6	11.8 - 37.6
<b>Zr</b>	0.41 $\pm$ 0.13	0.29 - 0.61	0.85 $\pm$ 0.24	0.48 - 1.06	0.51 $\pm$ 0.17	0.30 - 0.76

334

335 Generally, PM<sub>10</sub> concentrations are smaller in the month of May compared to June and July, as a  
336 consequence of an enhanced presence of winds at the ground resulting in longer ranges of dispersion of  
337 particulate matter.

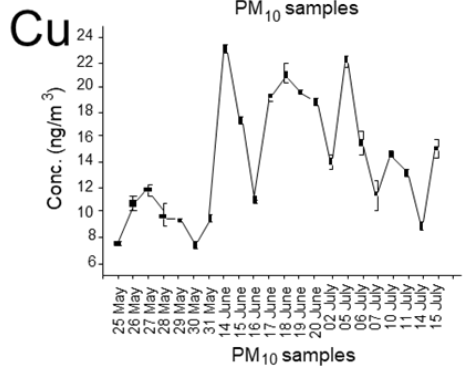
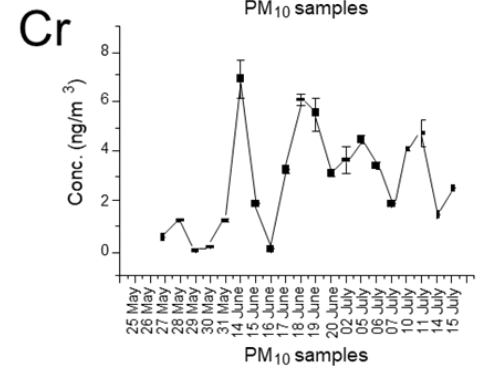
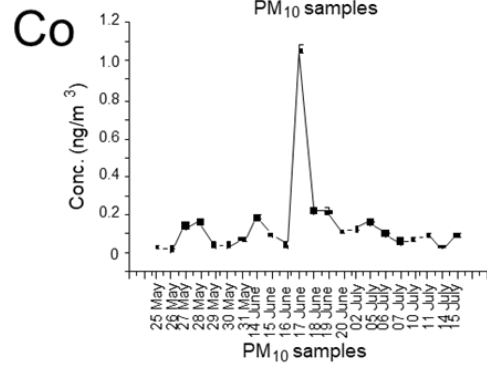
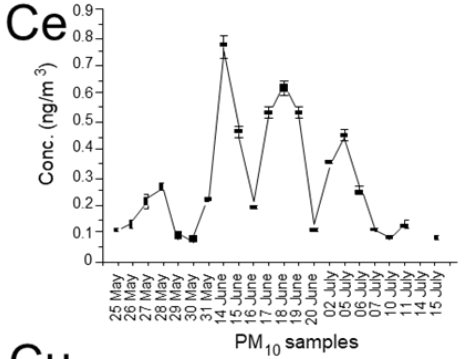
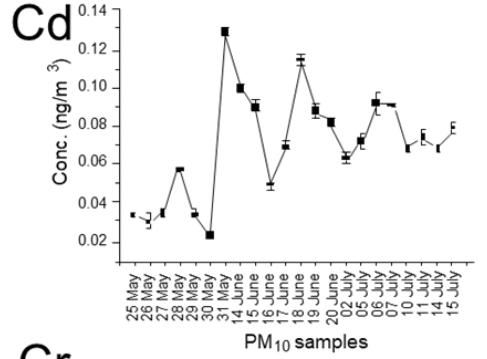
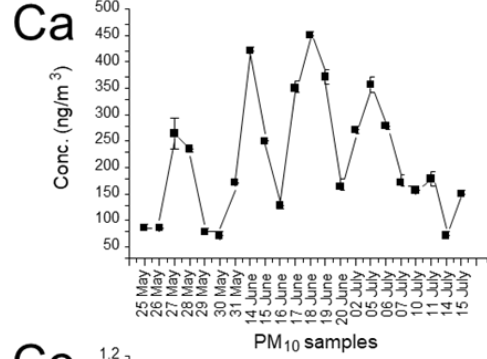
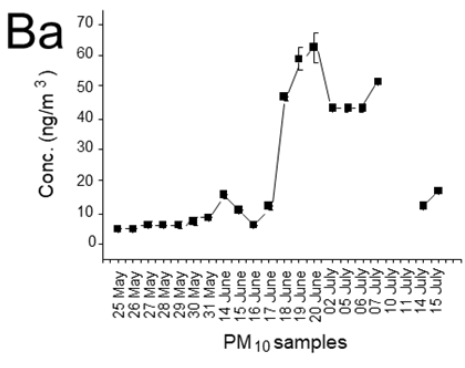
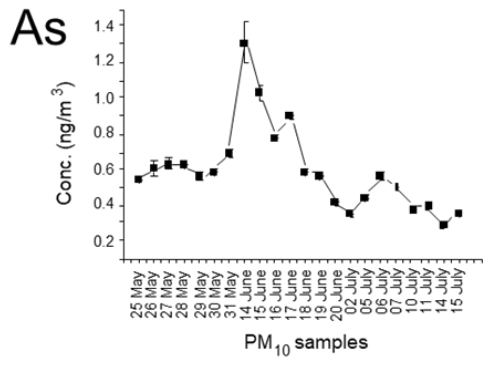
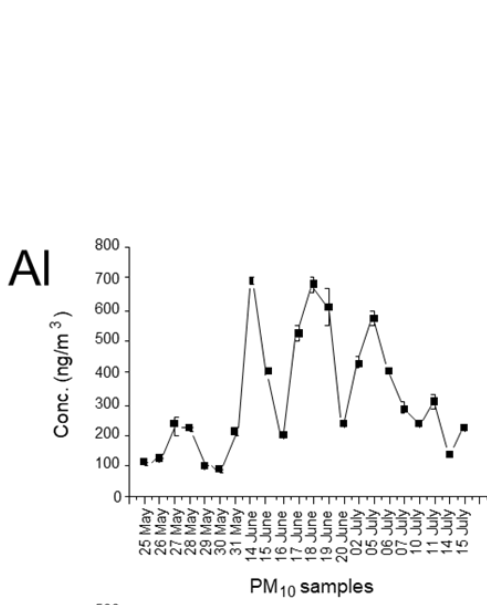
338 Regarding metal concentrations in PM<sub>10</sub>, the highest concentrations were found for the typically crustal  
339 elements, namely for Na, Al, Ca, Fe and Mg, clarifying the significant contribution of soil and re-suspended  
340 mineral particles to atmospheric PM, as reported in Padoan et al. (2016).

341 Considering the target values for As, Cd, Ni and the threshold value for Pb, reported in the European  
342 legislation (D. Lgs. 155, 2010), that are respectively 6, 5 and 20 ng/m<sup>3</sup> for the first three and 0.5 µg/m<sup>3</sup> for  
343 lead, it is notable that the concentrations of these analytes in all samples are one or two orders of magnitude  
344 lower than these values. These elements are the main targets for anthropogenic contributions, especially  
345 regarding combustion of fossil fuels and motor vehicles.

346 For trying to evaluate if the start-up phase of the incinerator resulted in an increase of the element  
347 concentrations in PM<sub>10</sub>, the element concentration trends have been considered (Figure 2). Overall, on the  
348 basis of the concentration trends, elements could be divided into three groups. Group 1 elements (As, Co,  
349 Na and V) show higher concentrations in May and June; Group 2 elements (Al, Ba, Ca, Ce, Cu, Fe, La,  
350 Mn, Ni, Ti, Zn and Zr) show an increase in their concentrations in June and at the beginning of July followed  
351 by a decrease around the middle of July; the concentrations of Group 3 elements (Cd, Cr, K, Mo, Pb, Sn  
352 and Tl) increase between May and June and remain almost constant in July.

353 As and V, belonging to the Group 1, are often referred to be emitted by incinerator plants (Sakata et al.,  
354 2000; Font et al., 2015), Na, instead, might derive from NaHCO<sub>3</sub>, used at the Turin incinerator plant for the  
355 abatement of acids from vapor emissions (<http://trm.to.it/>), the Co behavior is more difficult to explain  
356 because it is characterized by a very high concentration in 17 June sample but, to our knowledge, no  
357 particular event relating to the incinerator or, in general, to the air quality occurred on that date. It is  
358 noteworthy that from 22 May to 5 June the second combustion line was also put into operation for the first  
359 time and this could have led to the release of higher concentrations of Na and, to a lesser degree, As and V  
360 into the atmosphere.

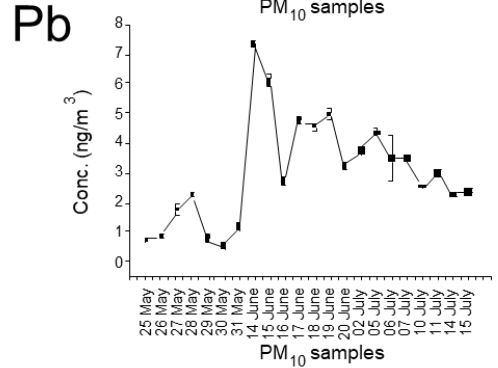
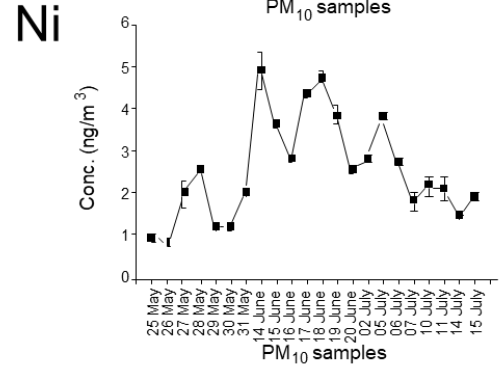
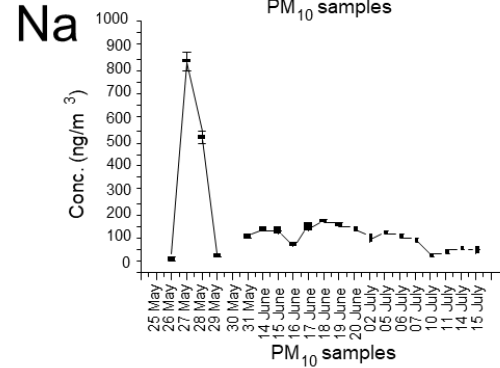
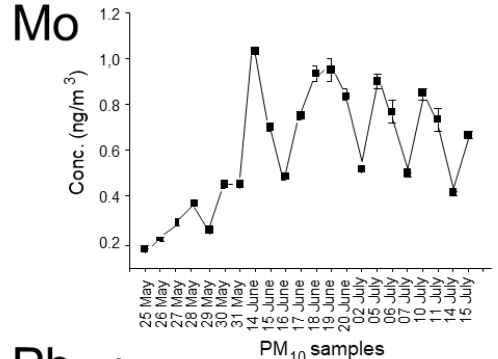
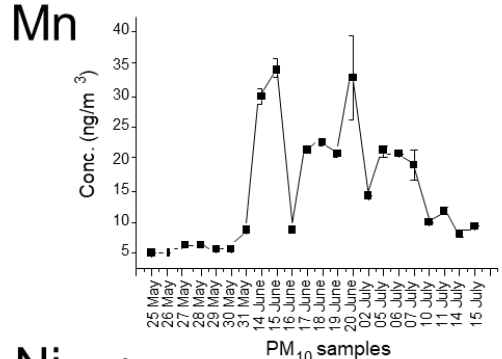
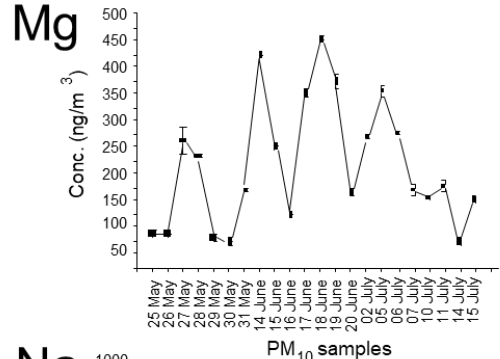
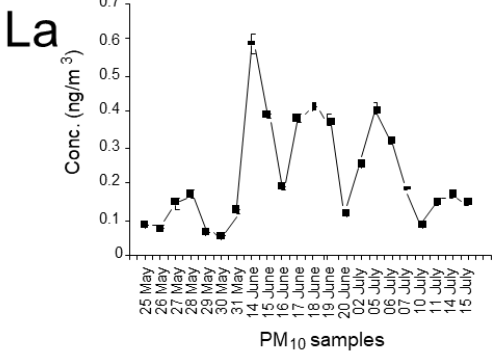
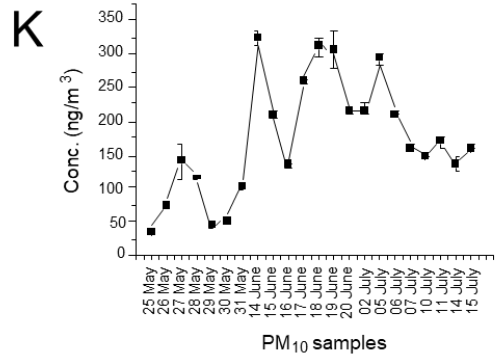
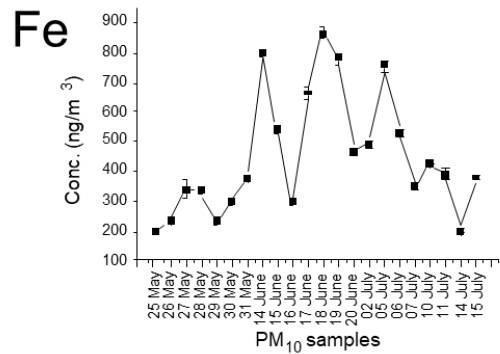
361 Most of the elements belonging to the Group 2 are typically geogenic, precisely Al, Ca, Ce, La, Ti and Zr.  
362 The same trend is also shown by Ba, Cu, Fe, Mn and Zn commonly associated also with non-exhaust vehicle  
363 emissions, as they are common indicators of release by mechanical abrasion of metal structures of vehicles,  
364 engine components, brake and tires wear and road dust (Birmili et al., 2006; Councell et al., 2004; Amato,  
365 2008). It is possible that between June and July, due to the start of the incinerator activities and the drier  
366 summer climate, proved also by the increase in temperatures recorded starting from mid-June, the road and  
367 soil dust resuspension phenomena are intensified, leading to enrichment of the typical elements of these  
368 sources in the PM<sub>10</sub>. Finally, the elements included in Group 3 are typically emitted during several  
369 combustion and industrial production processes: in particular Cd, Cr, Pb and Sn are also commonly  
370 associated with incinerator emissions (Pacyna et al.,2007; Font et al.,2015).

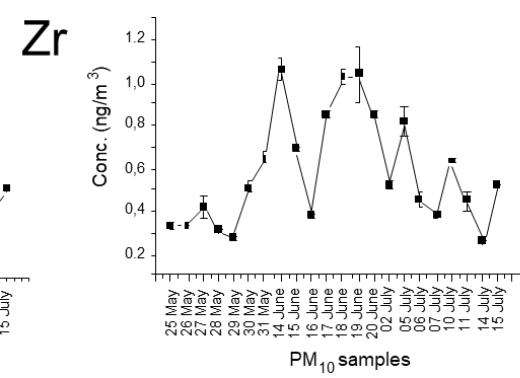
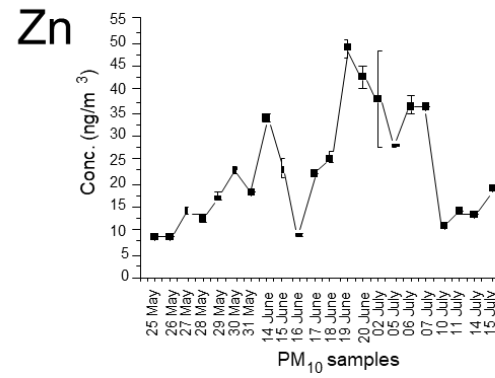
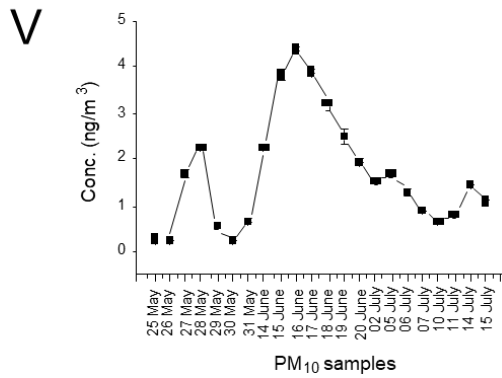
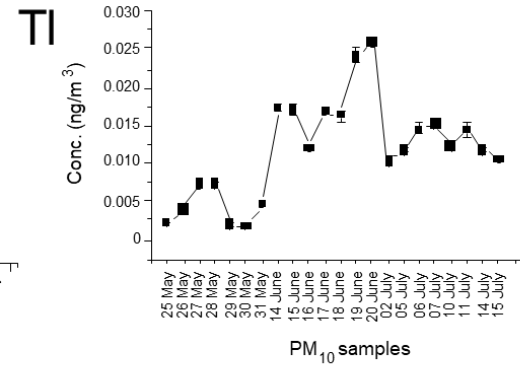
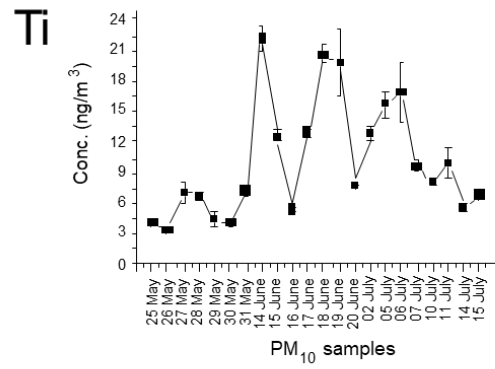
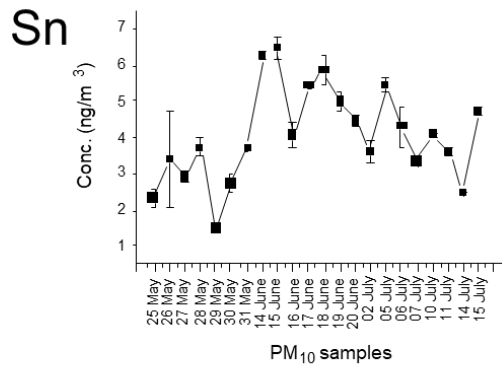


371

372

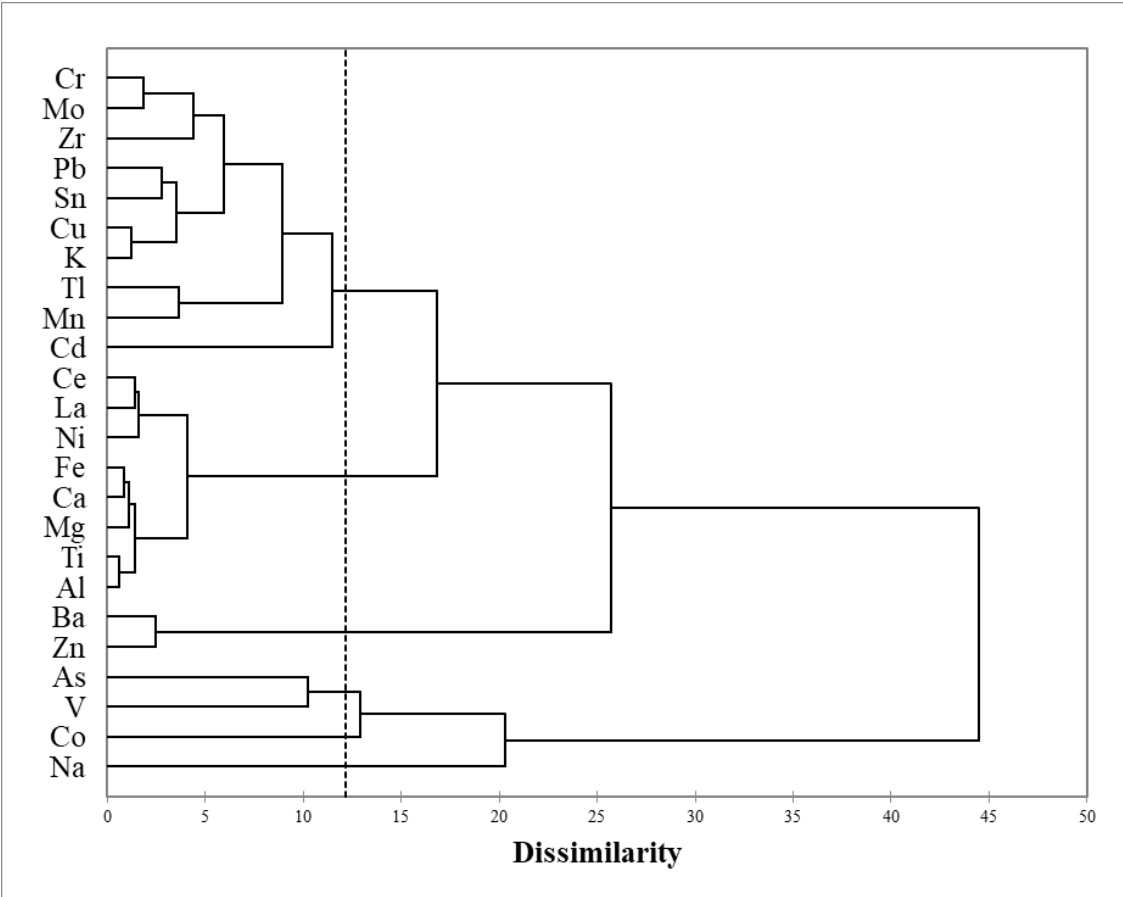
(continued)





376 *Figure 2: Element trends during start-up phase of the incinerator.*

377 In an effort to gain insight into the possible sources of PM<sub>10</sub>, a chemometric treatment of the experimental  
 378 data was carried out through the well-known Q-mode HCA in which we assume that different levels of  
 379 dissimilarity among elements are indicative of different emission sources (Figure 3).  
 380



381  
 382 *Figure 3: Dendrogram obtained by Q-mode HCA*

383  
 384 Starting from the bottom of the figure, the first cluster is composed by As, Co, Na and V, i.e. the elements  
 385 belonging to Group 1: they are linked at high levels of dissimilarity, suggesting that they do not derive from  
 386 a single emission source but they are likely all emitted in atmosphere from several anthropogenic sources,  
 387 probably attributable also to activities that have occurred in the start-up phase of the incinerator, such as  
 388 the temporary commissioning of the second combustion line. A second cluster is characterized by only two  
 389 elements, namely Ba and Zn; several researchers (Pakkanen et al., 2001; Malandrino et al. 2013; Zhang et



390 al. 2020) identified these elements as typical markers of road dust source because the former is added to  
391 lubricating oils to prevent smoke and diesel engine abrasion and the latter is also generated by dust caused  
392 by vehicular movement or exhaust emission. It is necessary to specify that generally these elements are also  
393 associated with crustal elements in identifying the road dust source, while here they are linked at high level  
394 of dissimilarity with these elements grouped together in a third cluster. This could be due to the fact that  
395 while crustal elements are enriched when the environmental conditions are favorable to the resuspension  
396 of soil dust, the resuspension of road dust occurred due to the heavier traffic of trucks carrying the wastes  
397 to the incinerator. As already mentioned, the third cluster is characterized by several elements, namely Al,  
398 Ca, Ce, Fe, La, Mg, Ni and Ti, that are linked at low levels of dissimilarity, suggesting a common source  
399 associated with soil dust. Finally the last cluster groups many elements, namely K, Cr, Cu, Mn, Mo, Pb, Sn,  
400 Tl and Zr, that are linked at different levels of dissimilarity, suggesting that they are emitted in atmosphere  
401 from several anthropogenic sources. In particular, the clustering of K, Cu, Pb and Sn could represent the  
402 direct incinerator emissions since Pb, Sn and Cu are commonly associated with this source and K is a  
403 common marker of biomass burning events (Lucarelli et al., 2019) while the other elements probably derive  
404 from city vehicular traffic and other industrial activities.

405 Overall, it is likely that the increase of concentrations for Ba, Cd, Cr, Cu, K, Mo, Pb, Sn and Zn during  
406 start-up phase of MSWI plant was caused by a combination of factors: the vehicular traffic, presumably  
407 increased in this area due to the commissioning of the incinerator, and a possible direct contribution deriving  
408 from the incinerator emissions; however, a contribution from the city vehicular traffic and industrial  
409 activities cannot be excluded.

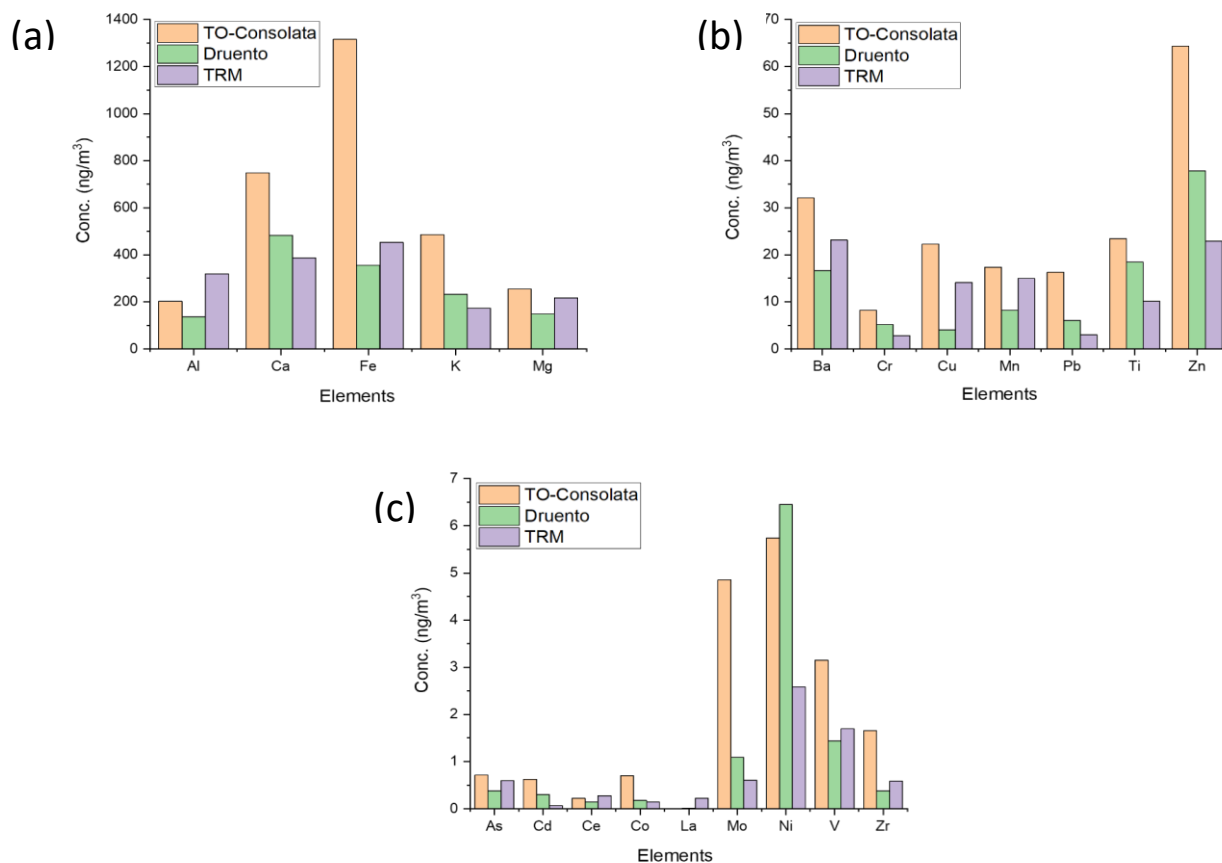
410 In this study, a comparison between results obtained in two nearby areas (Padoan et al., 2016) for an urban  
411 site (Torino-Consolata, TO-Consolata) and a rural site (Druento) in 2011 and in the same monitoring station  
412 between October and December in 2012 and 2014 was accomplished in order to identify a possible variation  
413 of PM sources and/or of their influence due to the MSWI start-up (Table 2). TO-Consolata site is localized  
414 in the historical centre of Turin and is mainly affected by vehicular traffic and heating emissions. Druento  
415 site is classified as a rural site by ARPA Piedmont and is localized in the small town of Druento, within a

416 regional park, with no direct influence of urban activities. This station is considered as a background site.  
417 In Figure 4 it is possible to notice the difference between the three sites for twenty-one elements having  
418 high (a), intermediate (b) and low (c) concentrations.

419 **Table 2.** Mean and standard deviation (Mean  $\pm$  SD), and 5<sup>th</sup> - 95<sup>th</sup> percentiles of each element determined in PM<sub>10</sub> samples collected in TRM site in 2013.  
 420 For comparison, descriptive statistics of the inorganic composition of the PM<sub>10</sub> collected in TRM site in 2012 and 2014 (Conca et al., 2020) and in TO-  
 421 Consolata and Druento sites in 2011 (Padoan et al., 2016) are also reported. All the concentrations are expressed in ng/m<sup>3</sup>.

	This study		2012 TRM		2014 TRM		2011 TO - Consolata		2011 Druento	
	Mean $\pm$ SD	5 <sup>th</sup> - 95 <sup>th</sup> perc.	Mean	5 <sup>th</sup> - 95 <sup>th</sup> perc.	Mean	5 <sup>th</sup> - 95 <sup>th</sup> perc.	Mean	Range	Mean	Range
Al	319 $\pm$ 192	102 – 677	170	33 - 470	250	98 - 530	203	17.8 - 428	137	4.08 - 531
As	0.60 $\pm$ 0.24	0.35 – 1.02	0.48	0.059 - 1.7	1.1	0.26 - 2.9	0.71	0.18 - 1.48	0.38	0.14 – 0.7
Ba	23 $\pm$ 21	4.8 – 58.8	48	19 - 150	52	40 - 78	32.1	12.4 – 76.9	16.7	7.39 – 54.5
Ca	387 $\pm$ 203	139 – 780	580	140 - 1200	1700	840 - 5000	749	18.7 – 1517	482	146 – 1460
Cd	0.07 $\pm$ 0.03	0.03 – 0.11	0.32	0.12 - 0.83	0.29	0.020 - 2.7	0.62	0.19 - 1.08	0.31	0.05 – 1.01
Ce	0.28 $\pm$ 0.21	0.08 – 0.62	0.33	0.076 - 0.66	0.34	0.16 - 0.65	0.22	0 - 0.88	0.15	0 – 1.53
Co	0.15 $\pm$ 0.21	0.036 – 0.22	0.32	0.036 - 1.1	0.31	0.082 - 0.64	0.7	0.06 - 1.85	0.18	0 – 0.87
Cr	2.8 $\pm$ 2.0	0.09 – 6.08	6.4	2.4 - 12	5.2	2.3 - 12	8.24	1.9 – 14.3	5.22	0.51 – 12.5
Cu	14.1 $\pm$ 4.9	7.55 – 22.0	40	7.8 - 79	27	11 - 77	22.3	5.04 – 52.4	3.9	0 – 15.1
Fe	453 $\pm$ 204	203 – 800	1200	260 - 2200	720	230 - 1700	1316	272 - 3164	356	57.4 – 658
K	174 $\pm$ 87	46 – 309	360	61 - 1100	860	330 - 2100	486	79.4 - 1285	232	56.8 – 472
La	0.22 $\pm$ 0.14	0.065 – 0.41	0.19	0.076 - 0.34	0.12	0.060 - 0.34	< 0.007	< 0.007	0.02	0 – 0.47
Mg	217 $\pm$ 117	74 – 421	190	44 - 460	290	170 - 600	254	19 - 738	148	6.77 – 314
Mn	15 $\pm$ 9	5.4 – 33	14	2.6 - 27	12	3.3 - 30	17.3	3.63 – 37.5	8.23	2.04 – 31.3
Mo	0.61 $\pm$ 0.26	0.22 – 0.96	3.4	1.6 - 7.3	3.4	1.1 - 7.3	4.86	0.83 – 16.02	1.09	0.24 – 3.03
Na	154 $\pm$ 192	27 – 538	136	29 – 360	758	172 – 2303	n.a.	n.a.	n.a.	n.a.
Ni	2.6 $\pm$ 1.2	0.96 – 4.8	4.1	0.58 - 9.3	7.7	2.9 - 25.3	5.74	0 – 16.2	6.45	0 – 41.9
Pb	3.0 $\pm$ 1.8	0.76 – 6.0	8.5	0 - 26	10	3.2 - 25	16.3	3.8 – 44.6	6.06	1.7 – 13.2
Ti	10 $\pm$ 6	4.0 – 20	19	1.9 - 51	16	5.0 - 34	23.5	2.29 – 54	18.5	4.99 – 33.7
V	1.7 $\pm$ 1.2	0.26 – 3.9	1.3	0.20 - 3.1	1.2	0.34 - 2.2	3.15	1.06 - 5.73	1.44	0.67 – 2.5
Zn	23 $\pm$ 12	8.7 – 42	68	19 - 160	130	45 - 390	64.3	19.6 - 164	37.9	4.81 – 79.3
Zr	0.58 $\pm$ 0.26	0.28 – 1.04	n.a.	n.a.	n.a.	n.a.	1.66	0.29 – 4.01	0.38	0 – 3.43

422 n.a.: not available



424 **Figure 4:** Concentrations of metals and metalloids in  $PM_{10}$  in TO-Consolata (urban), Druento (rural)  
 425 and TRM (sub-urban) sites. (a) high, (b) intermediate and (c) low concentrations.

426

427 Generally, the concentration of analytes in TRM site is in between with respect to the urban site and the  
 428 rural one. In the urban site higher concentrations of analytes deriving from anthropogenic activities were  
 429 measured, due to vehicular traffic and industrial and residential combustion processes.

430 On the other hand, Al, La and Ce concentrations are slightly higher in the TRM site than in the other two  
 431 locations. Since the most probable common source for these elements is represented by the Earth's crust,  
 432 their concentration is usually higher when soil dust resuspension events are more likely, that is when higher  
 433 speed of wind is observed, as reported in May month in TRM site.

434 TRM site is considered a sub-urban site. Indeed, concentrations of these target metals are quite high

435 compared to rural sites, but still they are comparable to other sub-urbans sites (Gholampour et al., 2016).  
436 Finally, the element concentrations in TRM site during start-up phase of the incinerator are comparable or  
437 lower than those found in PM<sub>10</sub> samples collected in the same monitoring station in 2012 and 2013. This  
438 mainly happens due to the frequent thermal inversions occurring during autumn and winter. These climatic  
439 phenomena have a relevant effect, particularly in orographically complex areas such as the Alpine arc  
440 surrounding the North-West sector of Piedmont. The stagnation of air in the valley floors, caused by severe  
441 thermal inversions in winter, gives rise to an accumulation of all pollutants. In some situations, when the  
442 thermal inversion is very strong while the foehn winds are weak, air recirculation is limited, resulting in  
443 intense urban pollution. These results underline the unquestionable role of meteorology in the evolution of  
444 pollutant concentrations in air and the overall low contribution of elements arising from MSWI plant also  
445 during the start-up phase.

446 Finally, in Table 3, we compare the total PM<sub>10</sub>, As, Cd, Ni and Pb concentrations found in PM<sub>10</sub> samples  
447 collected in Torino Consolata, Druento and TRM sites in all 2013 and in May – July quarters of 2014-2018.  
448 It is evident that the concentrations for these elements in TRM site are in between the other two sites (ARPA  
449 Piemonte, 2013a; ARPA Piemonte, 2013b; ARPA Piemonte, 2014; ARPA Piemonte, 2015; ARPA  
450 Piemonte, 2016; ARPA Piemonte, 2017; ARPA Piemonte, 2018).

451

452 **Table 3.** Concentrations (mean  $\pm$  standard deviation; min-max) of total PM<sub>10</sub> (expressed in  $\mu\text{g}/\text{m}^3$ ) as well as As, Cd,  
 453 Ni and Pb (expressed in  $\text{ng}/\text{m}^3$ ) in 2013 and in May – July quarters of 2014-2018 for TO-Consolata (urban), Druento  
 454 (rural) e TRM (sub-urban) sites.

Element	2013			2014-2018 (May-July)		
	TO-Consolata	Druento	TRM	TO-Consolata	Druento	TRM
PM <sub>10</sub>	40 $\pm$ 28	24 $\pm$ 16	33 $\pm$ 23	21 $\pm$ 7	18 $\pm$ 3	18 $\pm$ 7
	(5 – 144)	(5 – 101)	(4 – 110)	(5 – 46)	(5 – 71)	(4 – 45)
As	0.71 $\pm$ 0.03	0.71 $\pm$ 0.03	0.71 $\pm$ 0.03	0.7	0.7	0.7
	(0.7 – 0.8)	(0.7 – 0.8)	(0.7 – 0.8)	(0.7 – 0.7)	(0.7 – 0.7)	(0.7 – 0.7)
Cd	0.23 $\pm$ 0.34	0.12 $\pm$ 0.04	0.22 $\pm$ 0.16	0.1	0.1	0.1
	(0.1 – 1.2)	(0.1 – 0.2)	(0.1 – 0.6)	(0.1 – 0.1)	(0.1 – 0.1)	(0.1 – 0.1)
Ni	4.88 $\pm$ 2.50	1.59 $\pm$ 1.14	2.95 $\pm$ 1.63	2.7 $\pm$ 1.3	3.0 $\pm$ 5.4	2.3 $\pm$ 1.2
	(2 – 11)	(0.7 – 3.8)	(0.7 – 5.8)	(0.7 – 5.4)	(0.7 – 23)	(0.7 – 5.3)
Pb	10 $\pm$ 6	4.2 $\pm$ 2.5	8.9 $\pm$ 5.6	4.2 $\pm$ 0.8	2.1 $\pm$ 0.8	3.1 $\pm$ 1.3
	(4 – 26)	(1 – 9)	(2 – 21)	(3 – 6)	(1 – 4)	(1 – 6)

455

456 No significant differences can be evidenced by Kruskal-Wallis test (significance level: 95%) due to the  
 457 high variability of As, Cd, Ni and Pb concentrations in PM<sub>10</sub> samples, but it is however possible to make  
 458 some general considerations. More precisely, relative to the whole year 2013, arsenic concentrations are  
 459 similar in the three sites, while PM, cadmium and lead concentrations are higher in TO-Consolata site where  
 460 the traffic and combustion phenomena are prevalent. Ni concentrations in the urban site are approximately  
 461 thrice and twice higher than in the rural and sub-urban sites respectively. Considering, instead, the May-  
 462 July quarters in the 2014-2018 period, it is evident that Cd and As concentrations are similar in the three  
 463 sites, while Ni and Pb concentrations are lower in TRM site than in TO-Consolata site. Finally, relative to  
 464 Druento, the Pb concentrations are higher and Ni concentrations are lower in TRM site. The anomalous Ni

465 behavior can be explained taking into account that the Druento site is located in a large regional park and,  
466 therefore, in spring-summer it is more subject to episodes of soil dust resuspension that increase Ni  
467 concentrations in PM, due to the high background levels of this element in Piedmont soils (Biasioli et al.,  
468 2006; Bonifacio et al., 2010; Padoan et al., 2016); this is also confirmed by high variability of Ni  
469 concentrations in this site. The Pb behavior, instead, is a further confirmation of its possible anthropogenic  
470 input to the PM in TRM site. However, since Pb is one of the principal markers of incinerator emission, a  
471 further study of lead isotopic ratios was performed in order to identify the possible sources of lead in the  
472 airborne particulate matter collected in TRM site.

473 In addition, we compared our results with target metals found in PM<sub>10</sub> emitted from Municipal Solid Waste  
474 Incinerators (MSWI) located in UK (Font et al., 2015), where As, Cd, Cr, Cu, Pb, Mn, Ni and V were  
475 considered as target pollutants of MSWI emissions. In all cases, considering maximum values, the element  
476 concentrations near such plants are several orders of magnitude higher than in TRM site (e.g., Pb  
477 concentration is 7.35 ng/m<sup>3</sup> in this study and 200 µg/m<sup>3</sup> in MSWI sites in UK (Font et al., 2015). This  
478 demonstrates that incinerators of new installation have a lower impact on atmospheric particulate matter  
479 composition thanks to current legislation and up-to-date technologies.

480 Moreover, to evaluate if the incinerator installed near Turin city influenced the PM<sub>10</sub> composition, Cu/Pb,  
481 Cd/Cu, Cr/Pb, and Cd/Pb ratios were calculated and compared with the values reported for MSWI, rural  
482 and traffic emissions in Font et al. (2015). These ratios were used to discriminate between the different  
483 sources of potentially toxic metals in airborne particulate matter. Table 4 shows that average values of  
484 Cu/Pb, Cd/Cu and Cd/Pb calculated in this study are prevalently typical of traffic pollution. Therefore, we  
485 can assume that the major contribution in Cu, Pb and Cd to PM<sub>10</sub> collected in TRM site is due to the traffic  
486 instead of being originated from the emissions of the incinerator. The high value found for Cr/Pb ratio is  
487 probably due to a relevant natural contribution for chromium from soils: as reported above, Piedmont plains  
488 originated during past fluvio-glacial events and are therefore made of sediments, which partly derive from  
489 serpentinitic areas; this, as already documented by other researchers (Biasioli et al., 2006; Bonifacio et al.,  
490 2010; Padoan et al., 2016), causes high background levels of Ni and Cr in soils and in soil dust.

491

492 **Table 4.** Typical Cu/Pb, Cd/Cu, Cr/Pb and Cd/Pb ratios calculated in this study compared with rural situation, MWI  
493 and traffic pollution (Font et al., 2015).

Ratio	This study	MSWI	Rural	Traffic
Cu/Pb	4.62	0.83	0.51	2.38
Cd/Cu	0.005	0.14	0.026	0.007
Cr/Pb	0.81	0.56	0.13	0.28
Cd/Pb	0.023	0.08	0.013	0.017

494

495 Finally, Enrichment Factors (EFs) were calculated with respect to the mean values for the Earth’s upper  
496 crust reported by Wedepohl (1995), in order to distinguish elements having geologic or non-geologic origin.

497 The equation used is the following:

498 
$$EF_i = \frac{C_{i PM} / C_{r PM}}{C_{i crust} / C_{r crust}}$$

499 where  $C_{i PM} / C_{r PM}$  and  $C_{i crust} / C_{r crust}$  are the ratios between the concentration of the element  $i$  and the  
500 concentration of a reference element  $r$  respectively in the sample and in the upper crust; in this work, Al  
501 was selected as a reference element. By convention, EFs lower than 10 are taken as an indication that an  
502 element has a prevailing geogenic origin, EFs between 10 and 100 indicate a moderate enrichment and EFs  
503 higher than 100 indicate that the element (called “enriched”) has a prevailing non-geogenic origin (Lai et  
504 al., 2017; Tahri et al., 2017).

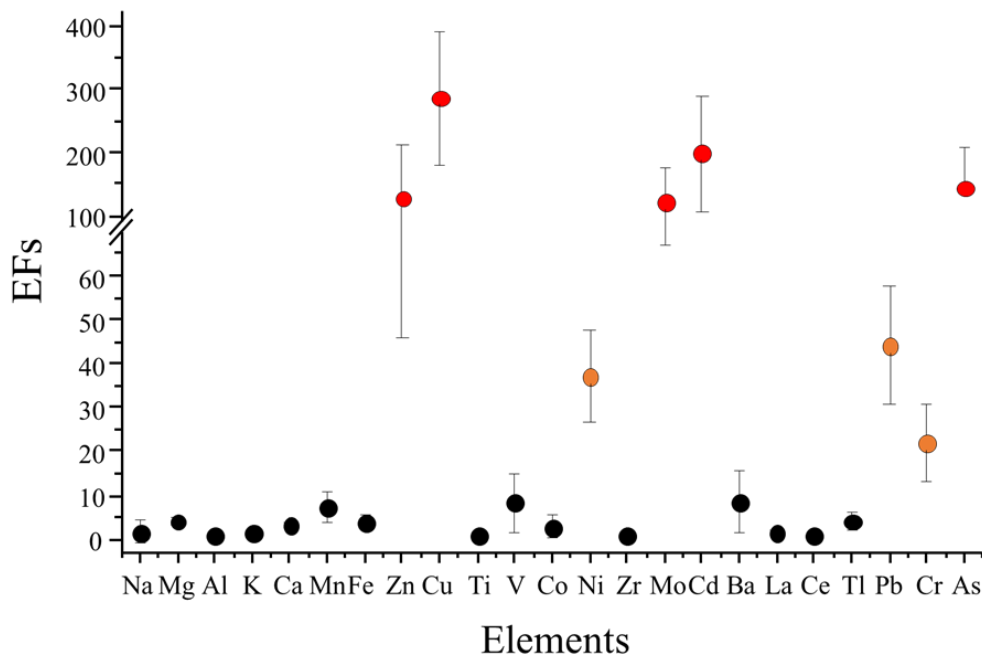
505 The average values of EFs were reported in Figure 5.

506

507

508





509

510 **Figure 5.** Enrichment Factors for elements determined in PM<sub>10</sub> samples.

511

512 As, Cd, Cr, Cu, Mo, Ni, Pb and Zn are predominantly generated by anthropic activities, with EFs values  
 513 higher than 10. These EFs are not higher than those reported for the city of Turin in previous studies (Padoan  
 514 et al., 2016), which represents a further confirmation that the installation of MSWI plant did not lead to an  
 515 increase in polluting emissions into the atmosphere. Finally, the elements moderately or highly enriched in  
 516 this sampling station can arise from vehicle emissions which likely increased in this area due to the opening  
 517 of the MSWI plant.

518

519 *3.1.2 Water-soluble ions concentrations*

520 The concentrations of major WSI and their contribution to the PM<sub>10</sub> concentrations are shown in Table 5,  
 521 where it can be seen that the respective average concentrations of the total WSI were 2.93, 8.87 and 5.16  
 522 µg/m<sup>3</sup> for May, June and July and accounted for 33.06%, 28.89% and 22.67% of the PM<sub>10</sub> mass. The average  
 523 percentage was equal to 28.21%, a percentage slightly lower compared to other studies (Ochsenkühn et al.,

524 2008; Li et al., 2015) where WSI is equivalent to 40%, but higher compared to a different work (Fan et al.,  
 525 2014), where WSI of 12% was measured. The concentrations of the WSI were dominated by  $\text{NO}_3^-$ ,  $\text{SO}_4^{2-}$   
 526 and  $\text{NH}_4^+$ , followed by  $\text{Ca}^{2+}$ ,  $\text{Na}^+$ ,  $\text{K}^+$ ,  $\text{Mg}^{2+}$  and  $\text{Cl}^-$ . It is also shown that secondary inorganic ions (SII:  
 527  $\text{NO}_3^-$ ,  $\text{SO}_4^{2-}$  and  $\text{NH}_4^+$ ) accounted for 77.37%, 89.13% and 87.98%, respectively, of the WSI for May, June  
 528 and July. In Table 5, it can be seen that the mean concentrations of the total WSI were higher in June and  
 529 July than in May: this is likely due to more consistent weather conditions in the two summer months.

530  
 531 **Table 5.** Mean and standard deviation (Mean  $\pm$  SD), and 5<sup>th</sup> - 95<sup>th</sup> percentiles of major water-soluble ions (WSI),  
 532 divided by month. All the concentrations are expressed in  $\text{ng}/\text{m}^3$  except  $\text{NH}_4^+$ ,  $\text{NO}_3^-$  and  $\text{SO}_4^{2-}$  which are expressed in  
 533  $\mu\text{g}/\text{m}^3$ .

Element	May		June		July	
	Mean $\pm$ SD	5 <sup>th</sup> - 95 <sup>th</sup> perc.	Mean $\pm$ SD	5 <sup>th</sup> - 95 <sup>th</sup> perc.	Mean $\pm$ SD	5 <sup>th</sup> - 95 <sup>th</sup> perc.
$\text{Cl}^-$	68 $\pm$ 110	19 – 234	20 $\pm$ 1	< 19 - 21	19 $\pm$ 1	< 19 – 21
$\text{NO}_3^-$	1.07 $\pm$ 0.9	0.48 – 2.48	4.8 $\pm$ 0.8	3.63 – 5.43	2.7 $\pm$ 0.5	2.23 – 3.53
$\text{SO}_4^{2-}$	0.90 $\pm$ 0.83	0.27 – 2.11	1.5 $\pm$ 0.5	0.81 – 2.03	0.83 $\pm$ 0.30	0.45 – 1.24
$\text{NH}_4^+$	0.30 $\pm$ 0.23	0.14 – 0.66	1.6 $\pm$ 0.2	1.34 – 1.94	0.99 $\pm$ 0.20	0.79 – 1.28
$\text{Ca}^{2+}$	203 $\pm$ 88	105 – 318	628 $\pm$ 196	351 – 830	411 $\pm$ 164	222 – 629
$\text{K}^+$	77 $\pm$ 22	46 – 103	134 $\pm$ 37	99 – 188	97 $\pm$ 19	78 – 123
$\text{Mg}^{2+}$	41 $\pm$ 43	10 – 107	57 $\pm$ 13	37 – 66	39 $\pm$ 12	23 – 54
$\text{Na}^+$	273 $\pm$ 383	29 – 873	125 $\pm$ 19	103 – 150	55 $\pm$ 16	33 – 73
SII	2266 $\pm$ 1916	922 – 5251	7909 $\pm$ 853	6816 – 9035	4538 $\pm$ 822	3729 – 5844
WSI	2928 $\pm$ 2475	1168 – 6654	8873 $\pm$ 825	7859 – 9981	5158 $\pm$ 883	4295 – 6525

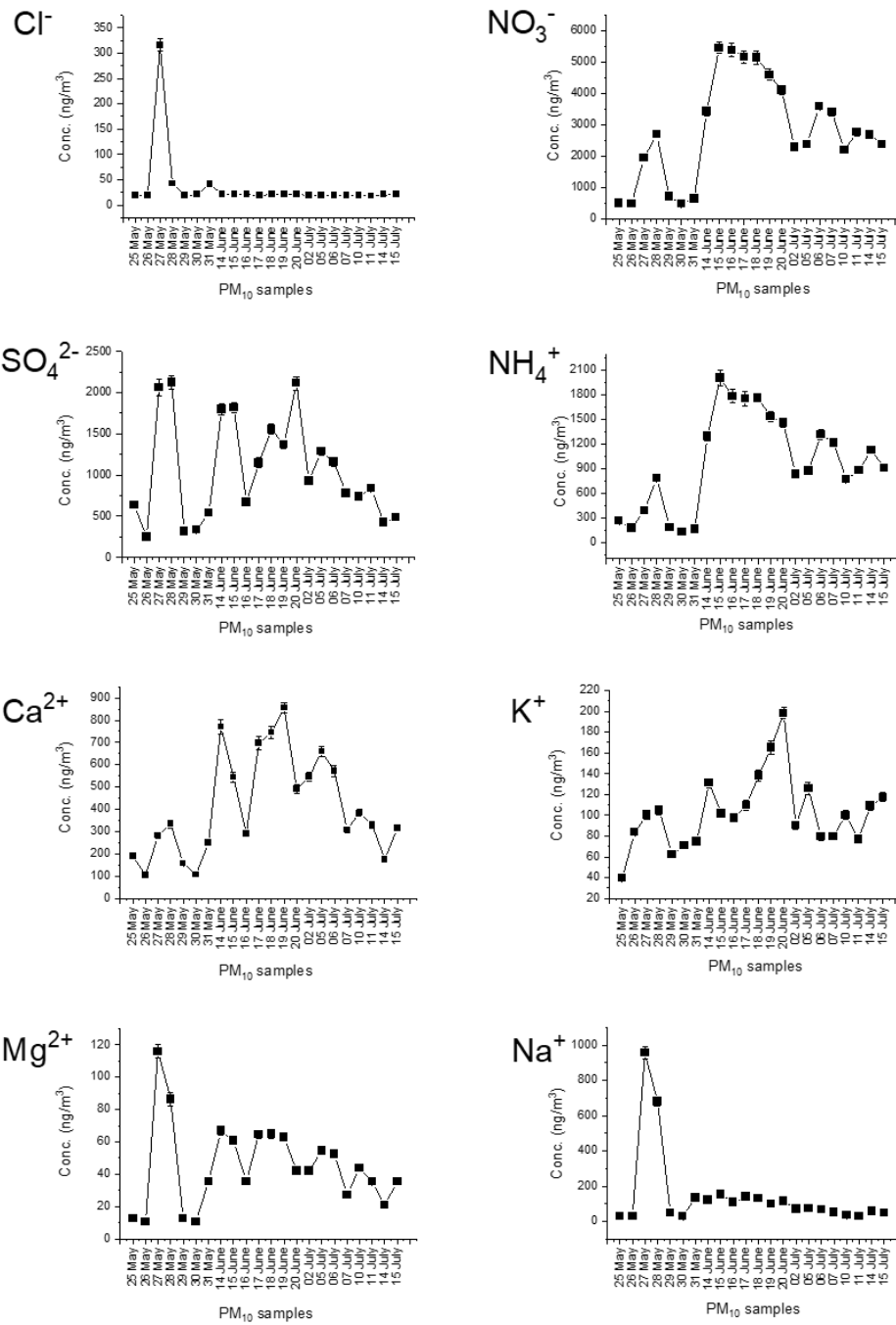
534  
 535 More in detail, anions content is larger compared to the cations one (19.70% vs 8.51%), prevalently  
 536 attributable to nitrates (13.08%) and sulfates (5.92%) produced by combustion processes in vehicles and  
 537 industries respectively. The main component of WSI is overall ammonium nitrate (Pearson's correlation  
 538 index between  $\text{NH}_4^+$  and  $\text{NO}_3^-$  is 0.985).

539 It has been reported that the mass ratio of nitrate/sulphate can be used to evaluate the relative contribution  
 540 of mobile and stationary sources in the atmosphere (Xu et al., 2012; Zhou et al., 2016). The mass ratios of

541  $\text{NO}_3^-/\text{SO}_4^{2-}$  in May, June and July were 1.19, 3.18 and 3.26 respectively; they were therefore greater than  
542 one, and this was especially true in June and July, which indicates that mobile sources (e.g. vehicle exhaust)  
543 make a greater contribution to aerosol pollution than stationary sources (e.g. incinerator). It should be noted  
544 that the mass ratios of  $\text{NO}_3^-/\text{SO}_4^{2-}$  increased greatly in the two summer months, which suggests that the  
545 vehicular traffic may have a more important effect on the  $\text{PM}_{10}$  concentration in the investigated area when  
546 the weather conditions are more stable.

547 Finally, higher concentrations of  $\text{Na}^+$  and  $\text{Cl}^-$  were found in May (Figure 6), when also the second  
548 combustion line of the incinerator was active. Direct incinerator emissions are conceivable sources for these  
549 ions: Na is used such as  $\text{NaHCO}_3$  at the Turin incinerator plant for the abatement of acids from vapor  
550 emissions (<http://trm.to.it/>) and, hence, it can combine with hydrochloric acid present in gaseous fumes  
551 arising from the combustion of organic chlorine present in waste (e.g. plastics, PVC, chlorinated solvents);  
552 NaCl can also be already present in the form of salt contained in paper and cardboard, food and vegetable  
553 waste. Moreover, it is interesting to note that, in May, when the NaCl concentration is higher, the  $\text{NH}_4\text{NO}_3$   
554 concentration is lower. This represents a further confirmation that NaCl is one of the main sinks of  $\text{NH}_4\text{NO}_3$   
555 in the aerosol (Ochsenkühn et al., 2008).

556



557

558 *Figure 6: Concentration trends during start-up phase of the incinerator for water-soluble ionic*  
 559 *components.*

560 **3.2 Optimization of instrumental parameters for Pb isotope ratios analysis**

561 The optimization of the experimental conditions of the instrumental parameters for Pb isotope ratios was  
562 carried out following the factorial design of experiments and response surface methodology, originally  
563 developed by Box and Wilson. In order to reduce the number of measurements we decide to perform a  
564 Central Composite Design (CCD) considering four instrumental parameters at the same time. In Table 6  
565 are reported the experimental parameters and the investigated ranges. A total of 24 different operative  
566 conditions plus 3 central points were considered.

567

568 **Table 6.** Investigated instrumental parameters and their range.

<i>INSTRUMENTAL PARAMETERS</i>	<i>LOW</i>	<i>INTERMEDIATE</i>	<i>HIGH</i>
Integration window (%)	60	80	100
Sampling points per peak	5	17	30
Run	1	5	9
Passes	1	5	9

569

570 Experiments were carried out randomly, both in low and medium resolution, using the two concentrations  
571 of SRM 981 standard (2.5 and 25 µg/L). Blank signal was subtracted for all the tests, and the interference  
572 of <sup>204</sup>Hg was considered with respect to <sup>204</sup>Pb by calculating mathematically the amount of this isotope after  
573 measuring <sup>202</sup>Hg that is not affected by any spectral interferences.

574 For each experiment the total accuracy was evaluated, that is the average of the absolute value of the  
575 accuracies for every isotope, together with the precision, that is the relative standard deviation of the  
576 accuracy for all the isotopes. Both accuracy and precision are expressed as percentages. Table 7 reports the  
577 results obtained for all the meaningful experiments in low and medium resolution, with the accuracy and  
578 the precision at SF-ICP-MS, at both 2.5 µg/L and 25 µg/L concentration of NIST SRM 981.

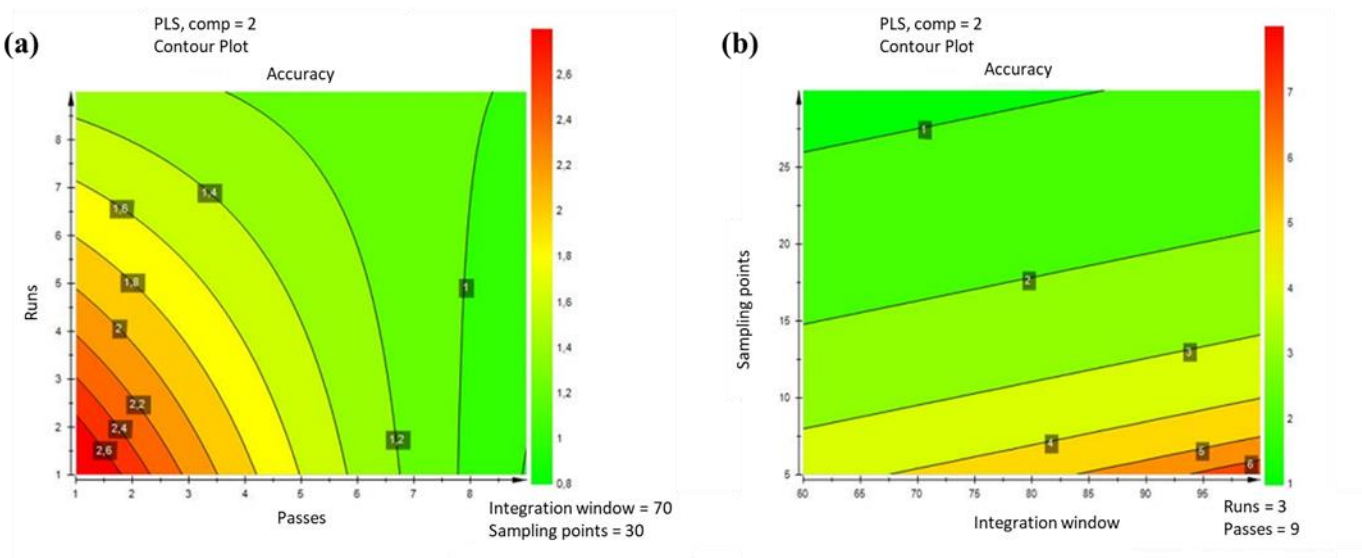
579

580 **Table 7.** Experiments set selected by CCD and carried out in LR (low resolution) and MR (medium resolution) for  
 581 the 2.5 and 25 µg/L of SRM981 concentration (results for experiments N2, N10, N13, N14 and N18 are not reported  
 582 because of the too low number of sampling points per peak).

Experiment	Accuracy	Precision	Accuracy	Precision	Accuracy	Precision	Accuracy	Precision
	2.5 µg/L	2.5 µg/L	25 µg/L	25 µg/L	2.5 µg/L	2.5 µg/L	25 µg/L	25 µg/L
	LR	LR	LR	LR	MR	MR	MR	MR
N1	2.59	2.05	5.45	6.8	17.35	8.34	11.29	13.05
N3	4.19	2.04	6.53	1.01	7.24	5.21	9.46	1.47
N4	4.77	5.64	2.73	1.77	7.06	6.01	1.2	0.41
N5	2.02	1.91	4.31	1.45	5.89	2.19	2.78	1.92
N6	9.84	11.02	2.28	3.11	8.6	8.93	4.55	0.17
N7	1.53	1.56	1.6	1.75	3.19	3.43	0.74	0.78
N8	1.05	1.2	1.62	1.62	1.66	0.86	3.94	1.33
N9	2.74	0.65	2.93	2.45	2.33	2.96	5.03	5.92
N11	0.83	0.97	1.95	2.01	2.73	3.17	1.32	0.52
N12	1.01	1.33	0.57	0.09	3.56	4.34	3.06	2.89
N15	1.06	1.06	1.05	1.06	0.82	0.98	0.96	0.75
N16	1.52	1.31	1.01	1.1	2.41	1.75	0.92	1.12
N17	1.24	1.14	1.24	1.54	0.94	0.75	0.95	0.73
N18	2.19	2.14	2.6	1.29	3.1	1.36	0.62	0.67
N20	1.46	1.44	0.74	0.84	4.91	2.76	5.77	2.53
N21	4.21	3.34	2.12	1.44	5.7	5.08	4.15	3.71
N22	0.8	0.94	1.97	1.02	3.77	1.7	0.87	0.77
N23	2.65	2.75	2.43	2	4.19	3.71	3.89	2.02
N24	1.63	1.75	1.26	1.49	1.21	1.46	1.05	0.83
N25	2.34	2.43	1.85	0.79	1.05	0.78	1.19	0.84
N26	3.64	1.33	2.77	2.16	1.35	1.7	2.96	0.72
N27	2.64	1.97	0.61	0.58	0.8	0.89	2.43	2.22

583  
 584 Four groups of tests (responses) were carried out, for the two concentrations of NIST SRM 981 (2.5 and 25  
 585 µg/L) in low and medium resolution. A PLS (Partial Least Square) regression was applied to obtain a  
 586 second-order model by projecting the predicted variables and the observable ones to a new space  
 587 considering accuracy, precision and the four variables aforementioned. Variables were scaled at unit

588 variance when the model was fitted. The results were used to provide the minimum values of accuracy and  
589 precision (expressed in percentages) depicted in green in Figure 7.



590  
591 **Figure 7:** The effect of runs and passes (a) and sampling points and integration window (b) on accuracy  
592 of lead isotope ratios determination.

593  
594 In this way we were able to identify the experimental conditions with the closer values to the certified one  
595 and with minimum dispersion.

596 Among the four variables, sample points per peak was the most important one respect to accuracy and  
597 precision. The optimum response was obtained using 2.5  $\mu\text{g/L}$  of SRM 981 concentration in low resolution.

598 The related optimal values of the four variables (3 runs, 9 passes, 70% of integration window and 30  
599 sampling points per peak) produced values equal to a  $0.83 \pm 0.46\%$  of accuracy and  $0.75 \pm 0.42\%$  of

600 precision. Those operative conditions were successfully used in the isotopic investigation of lead for the  
601  $\text{PM}_{10}$  samples.

602  
603 **3.3 Lead isotope ratios determination**

604 Lead concentration is low in all the samples analyzed, with values between 0.8 ng/m<sup>3</sup> (during May) and 7.4  
 605 ng/m<sup>3</sup> (during June). EFs are in the range between 26.4 and 71.9, indicating a slightly anthropogenic  
 606 contribution for Pb in the PM<sub>10</sub> samples.

607 Lead isotope ratios for all PM<sub>10</sub> samples (Tables 8 and 8S) were determined, by adopting the optimized  
 608 experimental conditions previously described (paragraph 3.3), in order to identify more accurately the  
 609 possible sources of this element in the investigated area.

610

611 **Table 8.** Mean and standard deviation (Mean ± SD), median, and 5<sup>th</sup> - 95<sup>th</sup> percentiles of the lead isotope ratios  
 612 (namely <sup>204</sup>Pb/<sup>206</sup>Pb, <sup>206</sup>Pb/<sup>207</sup>Pb and <sup>208</sup>Pb/<sup>206</sup>Pb ratios) according to the month.

<sup>204</sup> Pb/ <sup>206</sup> Pb	May	June	July
Mean ± SD	0.0532 ± 0.0008	0.0545 ± 0.0021	0.0514 ± 0.0013
Median	0.0532	0.0551	0.0508
5 <sup>th</sup> - 95 <sup>th</sup> perc.	0.0519 – 0.0540	0.0515 – 0.0566	0.0502 – 0.0533
<sup>206</sup> Pb/ <sup>207</sup> Pb	May	June	July
Mean ± SD	1.1595 ± 0.0066	1.1578 ± 0.0166	1.1766 ± 0.0325
Median	1.1601	1.1643	1.1908
5 <sup>th</sup> - 95 <sup>th</sup> perc.	1.1502 – 1.1670	1.1327 – 1.1711	1.1351 – 1.2102
<sup>208</sup> Pb/ <sup>206</sup> Pb	May	June	July
Mean ± SD	2.0347 ± 0.124	1.9952 ± 0.0581	1.9300 ± 0.0550
Median	2.0922	2.0176	1.9106
5 <sup>th</sup> - 95 <sup>th</sup> perc.	1.8507 – 2.1216	1.9059 – 2.0473	1.8806 – 2.0143

613

614 With a view to monitor accuracy together with precision of measurements, periodical readings of SRM 981  
 615 were performed.



616 With the aim to define which are the sources of lead in the PM<sub>10</sub> samples, the isotopic signature of each  
617 possible source for Pb should be known. This signature is a consequence of the mineral characteristic of  
618 the soil or of the material from which industrial lead was extracted. Generally, it was observed that  
619 atmospheric Pb was mainly influenced by traffic during the first part of Nineties of the twentieth century,  
620 followed by a mixed influence on traffic and industry during the 1995-1999 period. After 2000, when leaded  
621 gasoline was forbidden in Europe, the greatest part of atmospheric lead is coming from industrial activities  
622 (De la Cruz et al., 2009; Widory et al., 2004).

623 While each lead source has its own specific isotopic composition, it is useful to note that separate  
624 geochemical reservoirs are linked together and the final isotopic composition of lead results from mixing  
625 of many diverse sources.

626 Tropospheric lead, when is produced by anthropic activities, is mostly associated with the submicrometric  
627 aerosols that can be transported over long distances making thus the interpretation of lead isotopic data not  
628 easy (Flament et al., 2002).

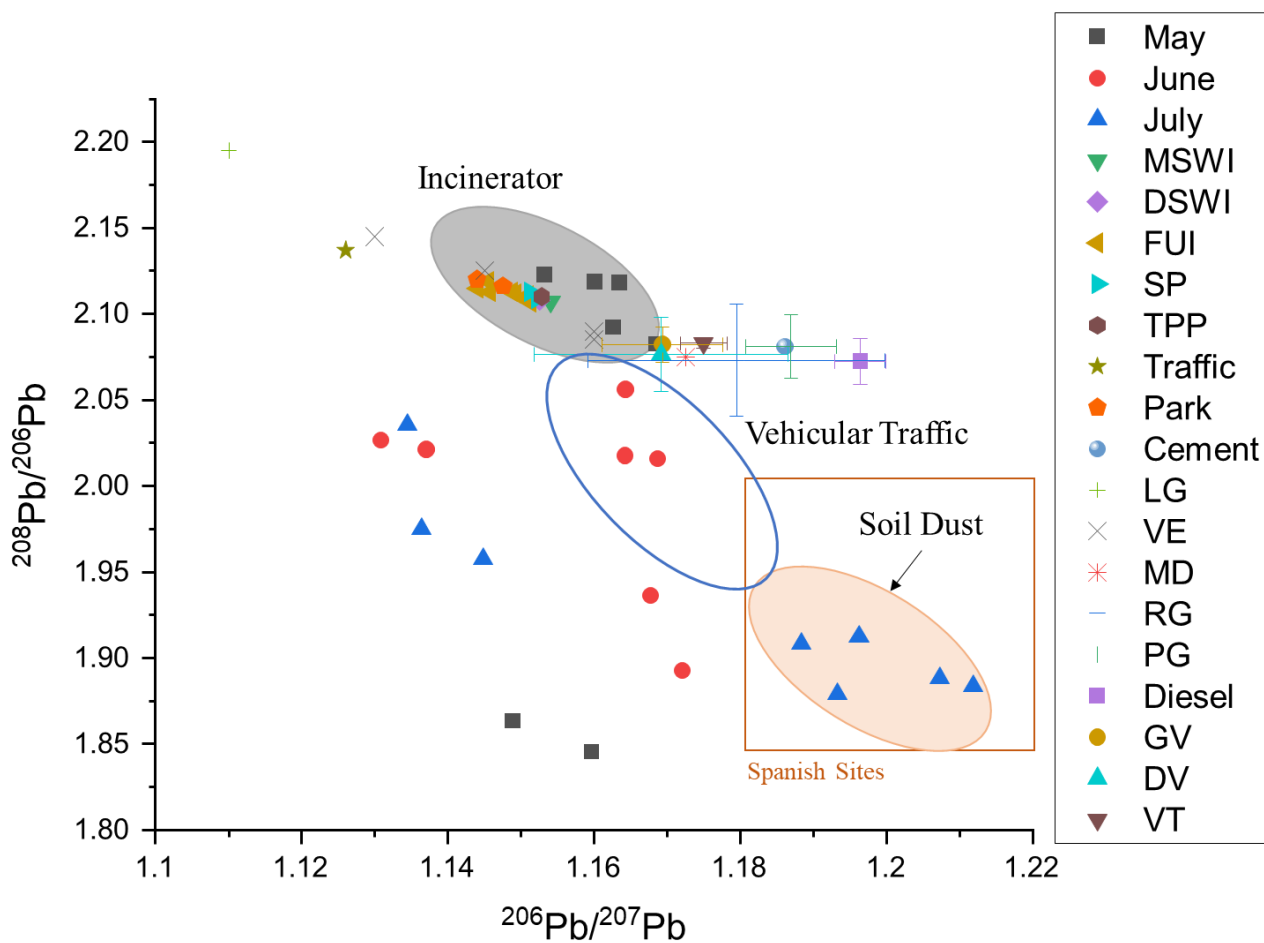
629 In addition, the isotopic composition of lead changes quickly depending on the different inputs for this  
630 element, distance from industrial areas, traffic density, prevailing wind directions and rainfall intensity  
631 (Simonetti et al., 2000).

632 In Europe, an important increase of the <sup>206</sup>Pb/<sup>207</sup>Pb ratio (from 1.09 to 1.17) was observed from the end of  
633 the 19<sup>th</sup> to the end of 20<sup>th</sup> century. This increase can be explained by several causes, such as a significant  
634 import of ores with less radiogenic ratios, modifications in industrial practices, combustion process of coal  
635 originating from different areas of the world (Bacon et al., 1996).

636 A further increase of the <sup>206</sup>Pb/<sup>207</sup>Pb ratio was caused by the introduction of leaded gasoline throughout the  
637 world. The subsequent decrease of the <sup>206</sup>Pb/<sup>207</sup>Pb ratio (to 1.09) in the 1980s reflects the gradual  
638 abandoning of leaded gasoline throughout Europe. These changes are associated with a decisive contraction  
639 of atmospheric lead concentrations.

640 Values obtained in this work for the lead isotopes, in terms of <sup>208</sup>Pb/<sup>206</sup>Pb and <sup>206</sup>Pb/<sup>207</sup>Pb ratios, are  
641 comparable to those found in the literature for countries from the Northern Hemisphere (De la Cruz et al.,

642 2009; Bollhöfer and Rosman, 2001) even if a higher radiogenic contribute was found respect to previous  
 643 works performed in Venice between 1998 and 1999. Firstly, in that case the concentration of lead was  
 644 higher (13-22 ng/m<sup>3</sup>) due to the presence of lead in gasoline in that period. Moreover, the values found for  
 645 <sup>208</sup>Pb/<sup>207</sup>Pb ratio (2.42-2.43) are comparable, denoting a variation only in the contribution of the radiogenic  
 646 isotope (<sup>206</sup>Pb) (Bollhöfer and Rosman, 2001).  
 647 Lead isotopic ratios determined in the PM<sub>10</sub> samples collected in TRM site are reported as <sup>208</sup>Pb/<sup>206</sup>Pb vs  
 648 <sup>206</sup>Pb/<sup>207</sup>Pb ratios in figure 8.



649  
 650 **Figure 8:** Plot of <sup>208</sup>Pb/<sup>206</sup>Pb vs <sup>206</sup>Pb/<sup>207</sup>Pb ratios for PM<sub>10</sub> samples collected in TRM site and in several  
 651 source samples from literature data: MSWI (Carignan et al., 2005); DSWI – Domestic Solid Waste  
 652 Incinerator, FUI – French Urban Incinerator, SP – Steel Plant, TPP – Thermal Power Plant, Traffic, Park,

653 *Cement (Lahd Geagea et al., 2008); LG – Loaded Gasoline, VE – Vehicle Exhaust, MD – Metallurgic Dust*  
654 *(Xu et al., 2020); RG – Regular Gasoline, PG – Premium Gasoline, Diesel, GV – Gasoline Vehicular, DV*  
655 *– Diesel Vehicular, VT – Vehicular Traffic (Gioia et al., 2017); Spanish Sites (Kylander et al., 2010).*

656  
657 A partial separation of July samples from May and June samples can be observed; most of the July samples,  
658 indeed, present low values for both  $^{206}\text{Pb}/^{207}\text{Pb}$  and  $^{208}\text{Pb}/^{206}\text{Pb}$  ratios. A distinction between May and June  
659 samples is not evident, even if May samples show intermediate values for the  $^{206}\text{Pb}/^{207}\text{Pb}$  ratios and a greater  
660 variability in the values for  $^{208}\text{Pb}/^{206}\text{Pb}$  ratios, whereas the June samples are characterized by higher values  
661 for the  $^{206}\text{Pb}/^{207}\text{Pb}$  ratios and intermediate values for  $^{208}\text{Pb}/^{206}\text{Pb}$  ratios.

662 Thus, comparing these results with other studies (Widory et al., 2004; Komárek et al., 2006; Novák et al.,  
663 2003; Teutsch et al., 2001; Carignan et al., 2005; Lahd Geagea et al., 2008; Guéguen et al., 2012; Gioia et  
664 al., 2010, 2017; Zhao et al., 2019; Lee et al., 2019; Xu et al. 2020), it is possible to speculate a principally  
665 geogenic contribution for lead in  $\text{PM}_{10}$  samples collected in July since the lead isotope ratios found in most  
666 of these samples are more characteristic of European ores. Indeed, the  $^{206}\text{Pb}/^{207}\text{Pb}$  ratios ranged from 1.8833  
667 to 1.2119, with an average value of 1.1994, similar to the results reported by Kylander et al. (2010),  
668 Kelepertzis et al. (2016) and Zhao et al. (2019), in which the natural end member of parent material showed  
669 higher  $^{206}\text{Pb}/^{207}\text{Pb}$  ratios compared with the anthropogenic-related sources. For example, the major soil dust  
670 emitting areas on a global scale, including the Sahara–Sahel area (Abouchami and Zabel, 2003), Gobi desert  
671 (Biscaye, et al., 1997) and European loess soils (Klaminder, et al., 2003; Sterckeman et al., 2006), have  
672  $^{206}\text{Pb}/^{207}\text{Pb}$  ratios varying between 1.19 and 1.25. The  $\text{PM}_{10}$  samples collected in June, instead, seem be  
673 more influenced by vehicular traffic ( $^{206}\text{Pb}/^{207}\text{Pb}$  ratios ranged from 1.1308 to 1.1721, with the average  
674 value of 1.1578). Indeed, these data fit well with  $^{206}\text{Pb}/^{207}\text{Pb}$  ratios determined by Gioia et al. (2010 and  
675 2017) for several traffic sources and suggest that the main source of lead in these samples is represented by  
676 vehicular traffic. Finally, it is particularly noteworthy that most of the  $\text{PM}_{10}$  samples collected in May  
677 display  $^{208}\text{Pb}/^{206}\text{Pb}$  and  $^{206}\text{Pb}/^{207}\text{Pb}$  ratios similar to values reported for several European MSWI plants

678 (Carignan et al, 2005; Geagea et al., 2008; Guéguen et al., 2012). The chemical and isotopic characterization  
679 of Pb emitted by MSWI plants is not an easy task because of the extreme heterogeneity of waste materials  
680 processed in these plants. Moreover, MSWI plants represent themselves a significant source of metals to  
681 the atmosphere. Nevertheless, the Pb isotopic composition for this source, reported in the literature  
682 (Carignan et al., 2005; Lahd Geagea et al., 2008 Guéguen et al., 2012), is fairly homogeneous and is defined  
683 by a restricted range in  $^{206}\text{Pb}/^{207}\text{Pb}$  and  $^{208}\text{Pb}/^{206}\text{Pb}$  values, 1.148-1.158 and 2.101-2.114 respectively,  
684 compared to other environmental samples. In conclusion, it is evident that the higher Pb content is not  
685 indicative of a greater contribution of this element to  $\text{PM}_{10}$  due to the MSWI commissioning because, during  
686 start-up phase, the lowest concentration for this element was observed in May (range: 0.54-2.27, mean:  
687 1.17  $\text{ng}/\text{m}^3$ ) and it increased in June and July (range: 2.73-7.35, mean: 1.58 in June and range: 2.26-4.36,  
688 mean: 3.16 in July). The commissioning of second line of combustion from 22 May to 5 June could be the  
689 most likely explanation for the greater influence of incinerator emissions on  $\text{PM}_{10}$ , evidenced by the Pb  
690 isotope ratios at the end of May. In July, when the MSWI plant has likely entered full capacity, it is possible  
691 that the Pb isotope ratios represent the typical sources influencing the  $\text{PM}_{10}$  in the investigated area, i.e.  
692 vehicular traffic and soil dust.

693

## 694 **Conclusions**

695

696 In conclusion, vehicular traffic was identified as the main atmospheric pollution source for  $\text{PM}_{10}$  samples  
697 collected near Turin MSWI plant. EFs and element concentrations are comparable with those reported for  
698 other sites located in the city of Turin confirming that the installation of MSWI plant did not lead to an  
699 overall increase in polluting emissions into the atmosphere. The elements moderately or highly enriched  
700 (Cr, Ni, Cu, Zn, As, Mo, Cd and Pb) seem to arise mainly from vehicle emissions which likely increased  
701 in this area after the opening of the MSWI plant due to heavier traffic of trucks carrying the wastes. This  
702 source of tropospheric pollution affects also lead concentration, as confirmed by lead isotope ratios

703 determined by a method that was developed and optimized using an experimental design approach..  
704 However, a possible crustal contribution in July and a possible influence of the incinerator in May have  
705 been highlighted taking into account the lead isotope ratios determined in PM<sub>10</sub> samples collected in these  
706 two months.  
707 Further studies about lead isotope ratios and PM<sub>10</sub> elemental composition should be done in the same area  
708 of sampling during incinerator activity for defining a possible long-term impact of the plant in the Turin  
709 suburban area.

710

## 711 **References**

712

713 Abouchami W., Zabel M., 2003. Climate forcing of the Pb isotope record of terrigenous input into the  
714 Equatorial Atlantic. *Earth Planet. Sci. Lett.* 213, 221–234. DOI: 10.1016/S0012-821X(03)00304-2.

715 Amato, F. *Non-exhaust emissions*; Elsevier: 2018.

716 Arpa Piemonte, *Rapporto di sintesi sui dati prodotti dalla stazione di monitoraggio della qualità dell'aria*  
717 *ubicata nel Comune di Beinasco – Giardino Pubblico Aldo Mei, di proprietà di TRM S.p.A. Anno 2013.*

718 Arpa Piemonte, 2013. *Uno sguardo all'aria.*

719 Arpa Piemonte, 2014. *Uno sguardo all'aria.*

720 Arpa Piemonte, 2015. *Uno sguardo all'aria.*

721 Arpa Piemonte, 2016. *Uno sguardo all'aria.*

722 Arpa Piemonte, 2017. *Uno sguardo all'aria.*

723 Arpa Piemonte, 2018. *Uno sguardo all'aria.*

724 Bacon J.R., Jones K.C., McGrath S.P., Johnston A.E., 1996. Isotopic character of lead deposited from the  
725 atmosphere at a grassland site in the United Kingdom since 1860. *Environ. Sci. Technol.* 30, 2511–2518.  
726 DOI: 10.1021/es950839s.

727 Biasioli M., Barberis R., Ajmone-Marsan F., 2006. The influence of a large city on some soil properties  
728 and metals content. *Sci. Total Environ.* 356, 154-164. DOI: 10.1016/j.scitotenv.2005.04.033.

729 Birmili W., Allen A.G., Bary F., Harrison R.M., 2006. Trace metal concentrations and water solubility in  
730 size-fractionated atmospheric particles and influence of road traffic. *Environ.Sci.Technol.* 40, 1144-1153.  
731 DOI: 10.1021/es0486925.

732 Biscaye P.E., Grousset F.E., Revel M., Gaast V.S., Zielinski G.A., Vaars A., Kukla G., 1997. Asian  
733 provenance of glacial dust (stage 2) in the Greenland Ice Sheet Project 2 ice core Summit Greenland. *J.*  
734 *Geophys. Res.* 102, 26765–26781. DOI: 10.1029/97JC01249.

735 Bollhöfer A., Rosman K.J.R., 2000. Isotopic source signatures for atmospheric lead: The Southern  
736 Hemisphere. *Geochim. Cosmochim. Acta* 64, 3251–3262. DOI: 10.1016/S0016-7037(00)00436-1.

737 Bollhöfer A., Rosman K.J.R., 2001. Isotopic source signatures for atmospheric lead: The Northern  
738 Hemisphere. *Geochim. Cosmochim. Acta.* 65, 1727-1740. DOI: 10.1016/S0016-7037(00)00630-X.

739 Bonifacio E., Falsone G., Piazza S., 2010. Linking Ni and Cr concentrations to soil mineralogy: does it help  
740 to assess metal contamination when the natural background is high? *J. Soils Sediments* 10, 1475-1486.  
741 DOI: 10.1007/s11368-010-0244-0.

742 Carignan J., Libourel G., Cloquet C., Le Forestier L., 2005. Lead isotopic composition of fly ash and flue  
743 gas residues from municipal solid waste combustors in France: implications for atmospheric lead source  
744 tracing. *Environ. Sci. Technol.* 39, 2018-2024. DOI: 10.1021/es048693x.

745 Cohen J., Cohen P., West S.G., Aiken L.S., 2003. *Applied multiple regression/correlation analysis for the*  
746 *behavioral sciences.* 3rd ed. Lawrence Erlbaum Associates, Inc., Mahwah, New Jersey.

747 Conca E., Malandrino M., Giacomino A., Inaudi P., Buoso S., Bande S., Sacco M., Abollino O., 2020.  
748 Contribution of the incinerator to the inorganic composition of the PM<sub>10</sub> collected in Turin, Atmosphere-  
749 Basel, 11, 400. DOI: 10.3390/atmos11040400.

750 Councill T.B., Duckenfield K.U., Landa E.R., Callender E., 2004. Tire-wear particles as a source of zinc  
751 to the environment. Environ. Sci. Technol., 38, 4206-4214. DOI: 10.1021/es034631f.

752 Decreto Ministeriale n 60 02/04/2002 from Council Directive 1999/30/EC of 22 April 1999.

753 De la Cruz M.T., Laborda F., Callén M.S., López J.M., Mastral A.M., 2009. Study of Pb sources by Pb  
754 isotope ratios in the airborne PM<sub>10</sub> of Zaragoza, Spain. J. Environ. Monit. 11, 2052-2057. DOI:  
755 10.1039/b912274e.

756 Directive 2000/76/EC of the European Parliament and of the Council of 28 December 2010 on the  
757 incineration of waste (the WI Directive).

758 Directive 2008/50/EC of the European Parliament and of the Council of 21 May 2008 on ambient air quality  
759 and cleaner air for Europe.

760 D.Lgs. 155, 2010. Official Gazette of the Italian Republic, 216.

761 European Environment Agency (EEA), 2013. Air quality in Europe – 2013 report 9/2013.

762 European Environment Agency (EEA), 2015. Air quality in Europe – 2015 report 5/2015.

763 Fan J., Yue X.Y., Jing Y., Chen Q., Wang S.G., 2014. Online monitoring of water-soluble ionic composition  
764 of PM<sub>10</sub> during early summer over Lanzhou City. J. Environ. Sci. 26, 353–361. DOI: 10.1016/S1001-  
765 0742(13)60431-3.

766 Flament P., Bertho M.L., Deboudt K., Veron A., Puskaric E., 2002. European isotopic signatures for lead  
767 in atmospheric aerosols: a source apportionment based upon Pb-206/Pb-207 ratios. Sci. Total. Environ.  
768 296, 35–57. DOI: 10.1016/S0048-9697(02)00021-9.

769 Font A., de Hoogh K., Leal-Sanchez M., Ashworth D.C., Brown R.J.C., Hansell A.L., Fuller G.W., 2015.  
770 Using metal ratios to detect emissions from municipal waste incinerators in ambient air pollution data.  
771 Atmos. Environ. 113, 177-186. DOI: 10.1016/j.atmosenv.2015.05.002.

772 Gao J.J., Tian H.Z., Cheng K., Lu L., Zheng M., Wang S.X., Hao J.M., Wang K., Hua S.B., Zhu C.Y.,  
773 Wang Y., 2015. The variation of chemical characteristics of PM<sub>2.5</sub> and PM<sub>10</sub> and formation causes during  
774 two haze pollution events in urban Beijing, China. Atmos. Environ. 107, 1-8. DOI:  
775 10.1016/j.atmosenv.2015.02.022.

776 Gerhardsson L., 2004. Lead In: Merian E., Anke M., Ihnat M., Stoepler M. (Eds.), Elements and their  
777 compounds in the environment, WILEY-VCH Verlag GmbH&Co. KGaA, Weinheim, 879-900.

778 Gholampour A., Nabizadeh R., Hassanvand M.S., Taghipour H., Rafee M., Alizadeh Z., Faridi S., Mahvi  
779 A.H., 2016. Characterization and source identification of trace elements in airborne particulates at urban  
780 and suburban atmospheres of Tabriz, Iran. Environ. Sci. Pollut. Res. Int. 23, 1703-1713. DOI:  
781 10.1007/s11356-015-5413-7.

782 Gioia, S.M.C.L., Babinski, M., Weiss, D.J., Kerr, A.A.F.S., 2010. Insights into the dynamics and sources  
783 of atmospheric lead and particulate matter in São Paulo, Brazil, from high temporal resolution sampling.  
784 Atmos. Res. 98, 478-485. DOI: 10.1016/j.atmosres.2010.08.016.

785 Gioia S.M.C.L., Babinski M., Weiss D.J., Spiro B., Kerr A.A.F.S., Veríssimo T.G., Ruiz I., Prates J.C.M.,  
786 2017. An isotopic study of atmospheric lead in a megacity after phasing out of leaded gasoline Atmos.  
787 Environ. 149, 70-83. DOI: 10.1016/j.atmosenv.2016.10.049.

788 Guéguen F., Stille P., Lahd Geagea M., Perrone T., Chabaux F., 2012. Atmospheric pollution in an urban  
789 environment by tree bark biomonitoring – Part II: Sr, Nd and Pb isotopic tracing, Chemosphere 86, 641–  
790 647. DOI: 10.1016/j.chemosphere.2011.11.008.



791 Harrison R.M., Jones A.M., Gietl J., Yin J., Green D.C., 2012. Estimation of the contributions of brake  
792 dust, tire wear, and resuspension to non-exhaust traffic particles derived from atmospheric measurements.  
793 Environ. Sci. Technol. 46, 6523-6529. DOI: 10.1021/es300894r.  
794 <http://trm.to.it/> (Date of access: 12 November 2020).  
795 <https://umetrics.com/product/modde> (Date of access: 20 October 2014).  
796 International Agency for Research on Cancer (IARC), 2012. IARC monographs on evaluation of  
797 carcinogenic risk of chemicals to humans. A review of human carcinogens: arsenic, metals, fibres, and  
798 dusts, Vol. 100 C. Lyon, France: World Health Organization.  
799 Kelepertzis E., Komárek M., Argyrakia A., Šillerová H., 2016. Metal(loid) distribution and Pb isotopic  
800 signatures in the urban environment of Athens, Greece. Environ. Pollut. 213, 420-431. DOI:  
801 10.1016/j.envpol.2016.02.049.  
802 Klaminder J., Renberg I., Bindler R., Emteryd O., 2003. Isotopic trends and background fluxes of  
803 atmospheric lead in northern Europe: analyses of three ombrotrophic bogs from south Sweden. Global  
804 Biogeochem. Cy. 17, 1019. DOI: 10.1029/2002GB001921.  
805 Komárek M., Chrastný V., Ettler V., Tlustoš P., 2006. Evaluation of extraction/digestion techniques used  
806 to determine lead isotopic composition in forest soils. Anal. Bioanal. Chem. 385, 1109–1115. DOI:  
807 10.1007/s00216-006-0543-x.  
808 Komarek M., Ettler V., Chrastný V., Mihaljevic M., 2008. Lead isotopes in environmental sciences: a  
809 review. Environ. Int. 34, 562-577. DOI: 10.1016/j.envint.2007.10.005  
810 Kylander M.E., Klaminder J., Bindler R., Weiss D.J., 2010. Natural lead isotope variations in the  
811 atmosphere. Earth Planet. Sc. Lett. 290, 44–53. DOI: 10.1016/j.epsl.2009.11.055.

812 Lahd Geagea M., Stille P., Gauthier - Lafaye F., Millet M., 2008. Tracing of industrial aerosol sources in  
813 an urban environment using Pb, Sr, and Nd isotopes. *Environ. Sci. Technol.* 42, 692–698. DOI:  
814 10.1021/es071704c.

815 Lai A.M., Shafer M.M., Dibb J.E., Polashenski C.M., Schauer J.J., 2017. Elements and inorganic ions as  
816 source tracers in recent Greenland snow. *Atmos. Environ.* 164: 205-215. DOI:  
817 10.1016/j.atmosenv.2017.05.048.

818 Lee S., Shin D., Han C., Choi K.S., Hur S.D., Lee J., Byun D.S., Kim Y.T., Hong S., 2019. Characteristic  
819 concentrations and isotopic composition of airborne lead at urban, rural and remote sites in western Korea.  
820 *Environ. Pollut.* 254, 113050. DOI: 10.1016/j.envpol.2019.113050.

821 Li T.C., Yuan C.S., Lo K.C., Hung C.H., Wu S.P, Tong C., 2015. Seasonal variation and chemical  
822 characteristics of atmospheric particles at three islands in the Taiwan strait. *Aerosol Air Qual. Res.* 15,  
823 2277–2290. DOI: 10.4209/aaqr.2015.03.0153.

824 Lucarelli F., Barrera V., Becagli S., Chiari M., Giannoni M., Nava S., Traversi R., Calzolari G., 2019.  
825 Combined use of daily and hourly data sets for the source apportionment of particulate matter near a waste  
826 incinerator plant. *Environ. Pollut.* 247, 802-811. DOI: 10.1016/j.envpol.2018.11.107.

827 Lundstedt T., Seifert E., Abramo L., Thelin B., Nystrom A., Pettersen J., Bergman R., 1998. Experimental  
828 design and optimization. *Chemom. Intell. Lab. Syst.* 42, 3-40.

829 Malandrino M., Di Martino M., Ghiotti G., Geobaldo F., Grosa M.M., Giacomino A., Abollino O., 2013.  
830 Inter-annual and seasonal variability in PM10 samples monitored in the city of Turin (Italy) from 2002 to  
831 2005. *Microchem. J.* 107, 76-85. DOI: 10.1016/j.microc.2012.05.026.

832 Meyer P.A., Brown M.J., Falk H. 2008. Global approach to reducing lead exposure and poisoning. *Mutat.*  
833 *Res. Rev. Mutat. Res.* 659, 166-175. DOI: 10.1016/j.mrrev.2008.03.003. Novák M., Emmanuel S., Vile  
834 M.A., Erel Y., Véron A., Pačes T., Wieder R.K., Vaněček M, Štěpánová M, Břízová E., Hovorka J., 2003.

835 Origin of lead in eight European peat bogs determined from isotope ratios, strengths, and operation times  
836 of regional pollution sources. *Environ. Sci. Technol.* 37, 437–445. DOI: 10.1021/es0200387.

837 Ochsenkühn K.M., Lyberopoulou T., Koumariou G., Ochsenkühn-Petropoulou M., 2008. Ion  
838 chromatographic and spectrometric determination of water-soluble compounds in airborne particulates, and  
839 their correlations in an industrial area in Attica, Greece. *Microchim. Acta.* 160, 485–492. DOI:  
840 10.1007/s00604-007-0830-z.

841 Pacyna E.G., Pacyna J.M., Fudala J., Strzelecka-Jastrzab E., Hlawiczka S., Panasiuk D., Nitter S., Pregger  
842 T., Pfeiffer H., Friedrich R., 2007. Current and future emissions of selected heavy metals to the atmosphere  
843 from anthropogenic sources in Europe. *Atmos. Environ.* 41, 8557e8566. DOI:  
844 10.1016/j.atmosenv.2007.07.040.

845 Padoan E., Malandrino M., Giacomino A., Grosa M., Lollobrigida F., Martini S., Abollino O., 2016. Spatial  
846 distribution and potential sources of trace elements in PM10 monitored in urban and rural sites of Piedmont  
847 Region. *Chemosphere* 145, 495–507. DOI: 10.1016/j.chemosphere.2015.11.094.

848 Pakkanen T., Loukkola K., Kohonen C., Aurela M., Mäkelä T., Hillamo, R., Aarnio P., Koskentalo T.,  
849 Kousa A., Maenhaut W., 2001. Sources and chemical composition of atmospheric fine and coarse particles  
850 in the Helsinki area. *Atmos. Environ.* 35, 5381-5391. DOI: 10.1016/S1352-2310(01)00307-7.

851 Panepinto D., Zanetti M.C., 2018. Municipal solid waste incineration plant: A multi-step approach to the  
852 evaluation of an energy-recovery configuration. *Waste Manage. (Oxford)* 73, 332-341, DOI:  
853 10.1016/j.wasman.2017.07.036.

854 Poschl U., 2005. Atmospheric aerosols. Composition, transformation, climate and health effects. *Angew.*  
855 *Chem. Int. Edit.* 44, 7520-7540. DOI: 10.1002/anie.200501122.

856 Raffaelli K., Deserti M., Stortini M., Amorati R., Vasconi M., Giovannini G., 2020. Improving air quality  
857 in the Po Valley, Italy: some results by the LIFE-IP-PREPAIR Project. *Atmosphere* 11, 429.  
858 DOI:10.3390/atmos11040429.

859 Rokach L., Maimon O., 2005. Clustering methods. Data mining and knowledge discovery handbook.  
860 Springer, Boston, US.

861 Sakata M., Kurata M., Tanaka, N., 2000. Estimating contribution from municipal solid waste incineration  
862 to trace metal concentrations in Japanese urban atmosphere using lead as a marker element. *Geochem. J.*  
863 34, 23-32. DOI: 10.2343/geochemj.34.23.

864 Simonetti A., Gariépy C., Carignan J., 2000. Pb and Sr isotopic compositions of snowpack from Québec,  
865 Canada: inferences on the sources and deposition budgets of atmospheric heavy metals. *Geochim*  
866 *Cosmochim. Acta* 64, 5–20. DOI: 10.1016/S0016-7037(99)00207-0.

867 Sterckeman T., Douay F., Baize D., Fourrier H., Proix N., Schwartz C., Carignan J., 2006. Trace element  
868 distributions in soils developed in loess deposits from northern France. *Eur. J. Soil Sci.* 57, 392–410. DOI:  
869 10.1111/j.1365-2389.2005.00750.x.

870 Tahri M., Benchrif A., Bounakhla M., Benyaich F., Noack Y., 2017. Seasonal variation and risk assessment  
871 of PM<sub>2.5</sub> and PM<sub>2.5-10</sub> in the ambient air of Kenitra, Morocco. *Environ. Sci.-Proc. Imp.* 19: 1427-1436.  
872 DOI: 10.1039/c7em00286f.

873 Teutsch N., Erel Y., Halicz L., Banin A., 2001. Distribution of natural and anthropogenic lead in  
874 Mediterranean soils. *Geochim. Cosmochim. Acta* 65, 2853–2864. DOI: 10.1016/S0016-7037(01)00607-X.

875 Tong S., von Schirnding Y.E.; Prapamontol T., 2000. Environmental lead exposure: a public health problem  
876 of global dimensions. *Bull. World Health Organ.* 78, 1068-1077.

877 Vinceti M., Malagoli C., Teggi S., Fabbi S., Goldoni C., De Girolamo G., Ferrari P., Astolfi G., Rivieri F.,  
878 Bergomi M., 2008. Adverse pregnancy outcomes in a population exposed to the emissions of a municipal  
879 waste incinerator. *Sci. Total Environ.* 407, 116–121. DOI: 10.1016/j.scitotenv.2008.08.027.

880 Wedepohl H., 1995. The composition of the continental crust. *Geochim. Cosmochim. Acta* 59, 1217-1232.

881 Widory D., Roy S., Le Moullec Y., Goupil G., Cocherie A., Guerrot C., 2004. The origin of atmospheric  
882 particles in Paris: a view through carbon and lead isotopes. *Atmos. Environ.* 38, 953–961. DOI:  
883 10.1016/j.atmosenv.2003.11.001.

884 Widory D., Liu X.D., Dong S.P., 2010. Isotopes as tracers of sources of lead and strontium in aerosols (TSP  
885 & PM<sub>2.5</sub>) in Beijing. *Atmos. Environ.* 44, 3679-3687. DOI: 10.1016/j.atmosenv.2010.06.036.

886 World Health Organization (WHO), 2007. Population health and waste management: scientific data and  
887 policy options. Report of a WHO workshop, Rome, Italy. Copenhagen, Denmark: Regional Office for  
888 Europe.

889 Xu L.L., Chen X.Q., Chen J.S., Zhang F.W., He C., Zhao J.P., Yin L.Q., 2012. Seasonal variations and  
890 chemical compositions of PM<sub>2.5</sub> aerosol in the urban area of Fuzhou, China. *Atmos. Res.* 104-105, 264-  
891 272. DOI: 10.1016/j.atmosres.2011.10.017.

892 Xu H.M., He K.L., Feng R., Shen Z.X., Cao J.J., Liu S.X., Ho K.F., Huang R.-J., Guinot B., Wang Q.Y.,  
893 Zhou J.M., Shen M. X., Xiao S., Zhouf B.H., Sonke J.E., 2020. Metallic elements and Pb isotopes in PM<sub>2.5</sub>  
894 in three Chinese typical megacities: spatial distribution and source apportionment. *Environ. Sci.: Processes*  
895 *Impacts* 22, 1718-1730. DOI: 10.1039/d0em00174k.

896 Yadav R., Sahu L.K., Jaaffrey S.N.A., Beig G., 2014. Distributions of ozone and related trace gases at an  
897 urban site in western India. *J. Atmos. Chem.* 71, 125–144. DOI: 10.1007/s10874-014-9286-9.

898 Zhang J., Peng J., Song C., Ma C., Men Z., Wu J., Wu L., Wang T., Zhang X., Tao S., Gao S., Hopke P.K.,  
899 Mao H., 2020. Vehicular non-exhaust particulate emissions in Chinese megacities: Source profiles, real-  
900 world emission factors, and inventories. *Environ. Pollut.* 266, 115268 DOI: 10.1016/j.envpol.2020.115268.

901 Zhao Y., Yu R.L., Hu G.R., Lin X.H., Liu X.R., 2017. Chemical characteristics and Pb isotopic  
902 compositions of PM<sub>2.5</sub> in Nanchang, China. *Particuology* 32, 95–102. DOI: 10.1016/j.partic.2016.07.009.

903 Zhao L., Hu G., Yan Y., Yu R., Cui J., Wang X., Yan Y., 2019. Source apportionment of heavy metals in  
904 urban road dust in a continental city of eastern China: Using Pb and Sr isotopes combined with multivariate  
905 statistical analysis. *Atmos. Environ.* 201, 201–211. DOI: 10.1016/j.atmosenv.2018.12.050.

906 Zhou J.B., Xing Z.Y., Deng J.J., Du K., 2016. Characterizing and sourcing ambient PM<sub>2.5</sub> over key  
907 emission regions in China I: water-soluble ions and carbonaceous fractions. *Atmos. Environ.* 135, 20-30.  
908 DOI: 10.1016/j.atmosenv.2016.03.054.

909 Zhou J.M., Shen M.X., Xiao S., Zhou B.H., Sonke J.E., 2020. Metallic elements and Pb isotopes in PM<sub>2.5</sub>  
910 in three Chinese typical megacities: spatial distribution and source apportionment. *Environ. Sci.-Proc. Imp.*  
911 22, 1718-1730. DOI: 10.1039/d0em00174k.

912 Zhu Y., Kashiwagi K., Sakaguchi M., Aoki M., Fujimori E., Haraguchi H., 2006. Lead isotopic  
913 compositions of atmospheric suspended particulate matter in Nagoya City as measured by HR-ICP-MS. *J.*  
914 *Nucl. Sci. Technol.* 43, 474-478. DOI: 10.3327/jnst.43.474.

## SUPPLEMENTARY MATERIAL

**Table 1S.** Meteorological data, PM<sub>10</sub> and PM<sub>2.5</sub> mass concentrations ( $\mu\text{g}/\text{m}^3$ ), and NO and NO<sub>2</sub> atmospheric concentrations ( $\mu\text{g}/\text{m}^3$ ) of the samples collected during start-up phase: a) from 09 May 2013 to 17 June 2013 and b) from 18 June 2013 to 16 July 2013.

a)	PM <sub>2.5</sub>	PM <sub>10</sub>	NO	NO <sub>2</sub>	WS avg (m/s)	WS max (m/s)	h avg (m)	h max (m)	T avg (°C)	b)	PM <sub>2.5</sub>	PM <sub>10</sub>	NO	NO <sub>2</sub>	WS avg (m/s)	WS max (m/s)	h avg (m)	h max (m)	T avg (°C)
<b>09/05</b>	n.a.	21	129	603	1.03	2.15	688	1419	19.08	<b>18/06</b>	22	36	74	677	0.68	1.07	618	1276	27.13
<b>10/05</b>	10	14	47	459	1.06	1.85	611	1305	16.31	<b>19/06</b>	21	33	64	618	0.73	1.23	547	1210	26.1
<b>11/05</b>	8	9	110	327	0.82	1.54	625	1370	17.27	<b>20/06</b>	17	27	131	784	0.92	1.77	559	1203	21.47
<b>12/05</b>	5	8	37	126	1.00	2.24	737	1465	17.79	<b>21/06</b>	15	21	104	485	0.86	1.42	700	1386	21.40
<b>13/05</b>	8	13	268	782	0.86	1.76	647	1316	16.56	<b>22/06</b>	12	18	65	411	1.07	1.58	732	1457	22.43
<b>14/05</b>	12	16	72	597	1.04	2.15	686	1380	16.17	<b>24/06</b>	4	10	62	503	1.15	2.82	837	1562	21.45
<b>15/05</b>	7	11	39	501	1.66	2.60	642	1281	12.08	<b>25/06</b>	5	8	152	1072	0.79	1.25	783	1567	20.58
<b>16/05</b>	3	6	99	620	1.83	2.73	562	1186	11.41	<b>26/06</b>	6	12	138	838	0.87	1.57	786	1555	20.55
<b>25/05</b>	5	5	46	336	1.34	2.47	567	1230	10.58	<b>27/06</b>	11	17	56	656	1.22	2.03	730	1462	17.44
<b>26/05</b>	6	5	71	438	1.19	1.74	631	1262	14.24	<b>28/06</b>	11	15	68	530	0.88	1.47	678	1401	16.46
<b>27/05</b>	9	11	99	509	1.16	2.54	607	1313	15.41	<b>29/06</b>	13	21	166	777	0.84	1.60	696	1433	18.22
<b>28/05</b>	11	20	77	396	0.88	1.79	561	1246	14.28	<b>30/06</b>	11	18	n.a.	593	0.85	1.65	705	1452	21.61
<b>29/05</b>	5	6	88	498	1.28	1.94	685	1360	12.37	<b>02/07</b>	12	23	101	476	0.76	1.66	790	1949	22.67
<b>30/05</b>	5	9	255	670	1.16	1.83	585	1279	14.32	<b>03/07</b>	14	21	n.a.	595	0.88	1.71	708	1444	21.00
<b>31/05</b>	6	6	235	598	1.28	1.86	602	1278	16.62	<b>04/07</b>	15	23	241	761	0.78	1.37	717	1422	23.40
<b>01/06</b>	9	14	102	433	0.87	1.42	594	1269	19.34	<b>05/07</b>	16	26	117	914	0.62	1.21	757	1507	25.30
<b>02/06</b>	7	49	58	422	0.88	1.43	726	1438	21.14	<b>06/07</b>	18	27	42	490	0.87	1.92	725	1492	25.36
<b>03/06</b>	16	19	n.a.	849	0.79	1.50	670	1320	18.27	<b>07/07</b>	15	21	11	326	1.08	1.63	658	1405	25.31
<b>04/06</b>	15	21	132	942	0.69	1.05	630	1236	19.17	<b>08/07</b>	15	22	93	490	0.76	1.36	662	1376	24.65
<b>05/06</b>	18	26	102	923	0.64	1.44	601	1326	19.14	<b>09/07</b>	11	16	117	542	0.81	1.27	592	1301	23.86
<b>08/06</b>	14	21	76	652	0.81	1.93	579	1297	20.22	<b>10/07</b>	13	21	123	815	0.62	1.10	666	1383	24.39
<b>09/06</b>	8	13	42	303	1.16	2.50	607	1209	15.33	<b>11/07</b>	14	23	56	553	0.74	1.79	711	1388	25.23
<b>10/06</b>	8	11	119	522	0.83	1.31	587	1220	17.59	<b>12/07</b>	18	29	48	529	0.75	1.95	682	1326	23.71
<b>11/06</b>	9	15	181	909	0.67	1.21	678	1400	21.14	<b>13/07</b>	21	31	n.a.	466	0.85	1.66	671	1293	24.22
<b>14/06</b>	20	33	68	735	0.83	1.75	730	1380	23.73	<b>14/07</b>	16	19	32	316	0.70	1.23	639	1370	23.95
<b>15/06</b>	21	32	51	548	1.02	2.05	739	1459	23.50	<b>15/07</b>	17	22	187	708	0.51	0.91	663	1428	25.24
<b>16/06</b>	16	23	45	331	1.03	1.50	719	1417	24.38	<b>16/07</b>	20	27	43	470	0.94	1.69	649	1375	24.95
<b>17/06</b>	19	31	107	729	0.67	1.14	615	1255	26.18										

WS avg = average wind speed; WS max = maximum wind speed; WD = wind direction; h avg = average mixing height; h max = maximum mixing height; T avg = average temperature.

**Table 2S.** Experimental conditions, limits of detection (LOD) and sample blank concentrations of the analytes determined by ICP-AES.

Analyte	LOD ( $\mu\text{g/L}$ )	Sample Blank A ( $\mu\text{g/L}$ )	Sample Blank B ( $\mu\text{g/L}$ )
Al 396.153	8.1	45	46
Ca 317.933	40.8	100	90
Fe 238.204	39.8	< LOD	< LOD
K 769.896	5.2	30	20
Mg 285.213	8.6	32	31
Mn 257.610	0.22	2.1	1.0
K 769.896	5.2	30	20

A: Millipore© filters; B: Munktell filters

**Table 3S.** Experimental conditions, limits of detection (LOD) and sample blank concentrations of the analytes determined by SF-ICP-MS

Analyte	LOD (ng/L)	Sample Blank A (ng/L)	Sample Blank B (ng/L)
Ti47(LR)	754	3,860	1,030
V51(LR)	12	58	90
Cr53(LR)	48	834	760
Co59(MR)	7.0	8.7	< LOD
Ni60(MR)	41	240	350
Cu63(LR)	583	< LOD	< LOD
Zn66(MR)	1,450	3,860	3,220
As75(LR)	13	< LOD	< LOD
Sn118(LR)	3.0	< LOD	< LOD
Zr90(LR)	12	660	620
Mo96(MR)	21	390	340
Cd111(LR)	6.0	9.6	< LOD



Ba138(LR)	253	910	1,360
La139(MR)	5.7	62	60
Ce140(MR)	2.0	260	300
Tl203(MR)	14	< LOD	< LOD
Pb208(LR)	13	68	53

LR = Low Resolution; MR = Medium Resolution; A: Millipore© filters; B: Munktell filters

**Table 4S.** Limits of detection (LOD) and sample blank concentrations of water-soluble ions determined by IC.

Analyte	LOD (µg/L)	Sample Blank A (µg/L)	Sample Blank B (µg/L)
Cl <sup>-</sup>	50	< LOD	< LOD
NO <sub>3</sub> <sup>-</sup>	500	< LOD	< LOD
SO <sub>4</sub> <sup>2-</sup>	800	< LOD	< LOD
Na <sup>+</sup>	250	< LOD	< LOD
K <sup>+</sup>	200	< LOD	< LOD
Mg <sup>2+</sup>	150	< LOD	< LOD
Ca <sup>2+</sup>	900	< LOD	< LOD
NH <sub>4</sub> <sup>+</sup>	100	< LOD	< LOD

A: Millipore© filters; B: Munktell filters

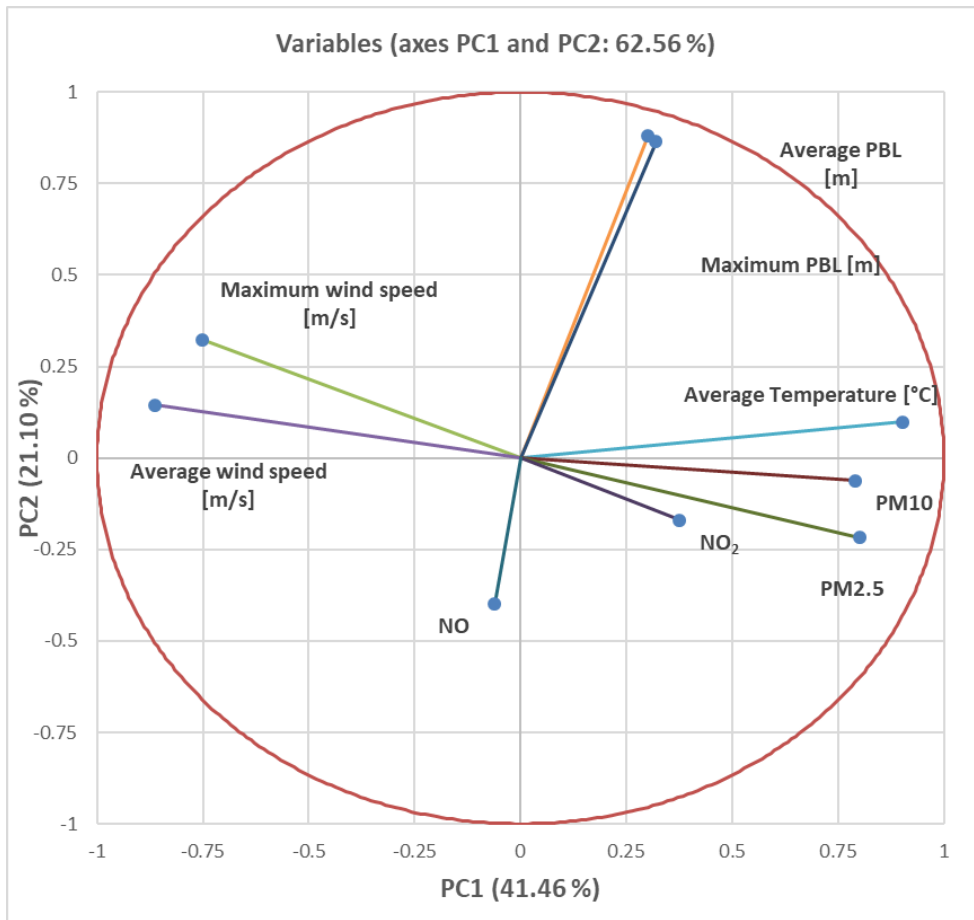


**Figure 1S.** Loadings from PCA (Principal Components Analysis).

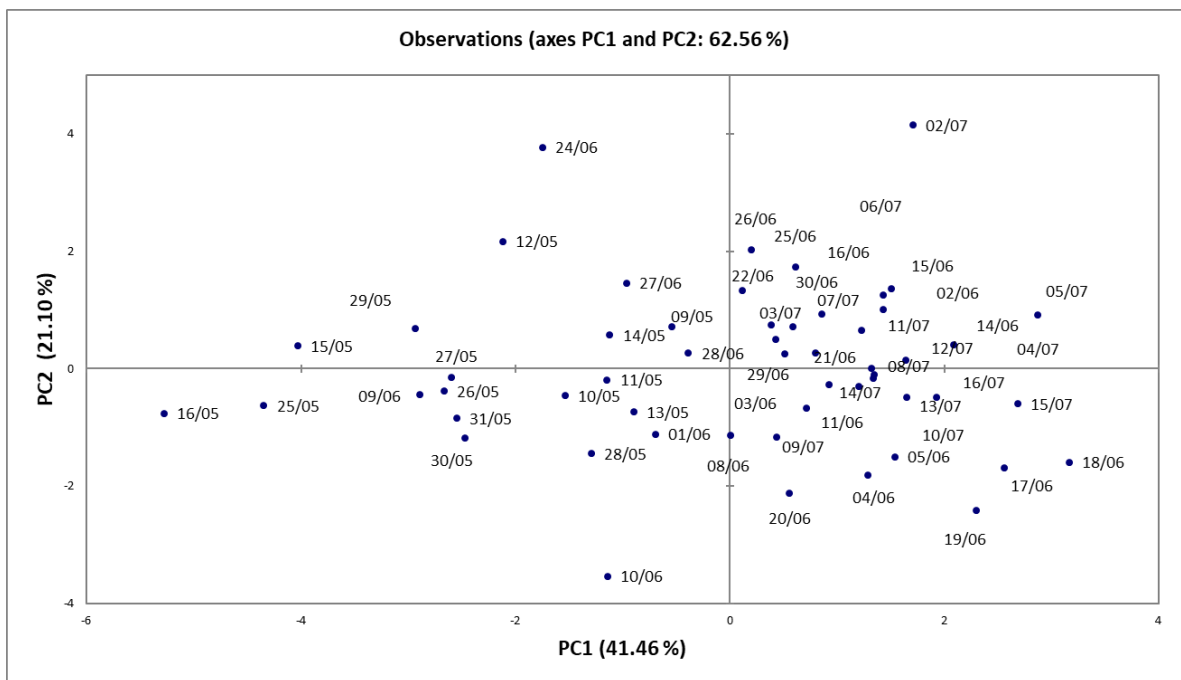


**Figure 2S.** Scores from PCA (Principal Components Analysis).

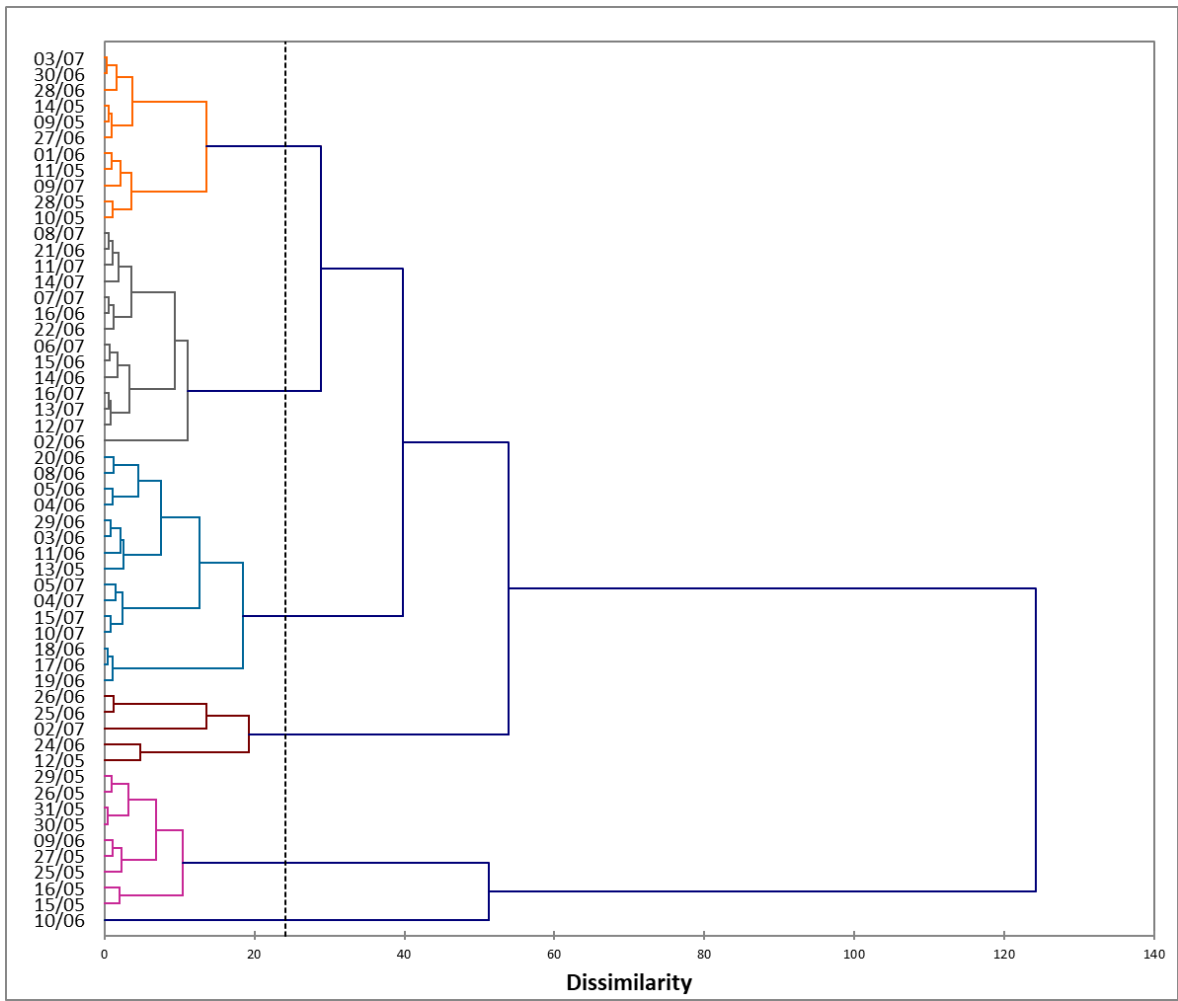


**Figure 3S.** Dendrogram of the samples from HCA (Hierarchical Cluster Analysis).

**Table 5S.** Water-soluble ionic components and major element concentrations in PM<sub>10</sub> samples. All the results are expressed in ng/m<sup>3</sup>, except NH<sub>4</sub><sup>+</sup>, NO<sub>3</sub><sup>-</sup> and SO<sub>4</sub><sup>2-</sup> which are expressed in µg/m<sup>3</sup>.

	Al	Ca	Ca <sup>2+</sup>	Cl <sup>-</sup>	Fe	K	K <sup>+</sup>	Mg	Mg <sup>2+</sup>	Na	Na <sup>+</sup>	NH <sub>4</sub> <sup>+</sup>	NO <sub>3</sub> <sup>-</sup>	SO <sub>4</sub> <sup>2-</sup>
<b>25 May</b>	108 ± 1	178 ± 7	191 ± 8	< 19	200 ± 3	36 ± 2	40 ± 2	88 ± 2	12.7 ± 0.4	< SB	31 ± 1	0.26 ± 0.01	5.1 ± 0.2	0.64 ± 0.02
<b>26 May</b>	127 ± 4	147 ± 5	103 ± 3	< 19	233 ± 1	76.5 ± 0.2	84 ± 3	85.8 ± 0.2	10.6 ± 0.5	15 ± 5	29 ± 1	0.17 ± 0.01	4.9 ± 0.2	0.253 ± 0.007
<b>27 May</b>	230 ± 30	350 ± 40	280 ± 10	320 ± 10	340 ± 30	140 ± 20	100 ± 4	260 ± 30	116 ± 4	840 ± 30	950 ± 40	0.39 ± 0.01	19.6 ± 0.9	2.1 ± 0.1
<b>28 May</b>	217 ± 4	340 ± 20	330 ± 20	42 ± 1	332 ± 5	117 ± 3	105 ± 4	230 ± 4	86 ± 4	520 ± 20	680 ± 20	0.78 ± 0.02	27 ± 1	2.13 ± 0.08
<b>29 May</b>	101 ± 3	175 ± 2	156 ± 6	< 19	235 ± 8	46 ± 5	63 ± 2	81 ± 4	12.7 ± 0.5	27 ± 1	50 ± 2	0.180 ± 0.007	7.2 ± 0.3	0.32 ± 0.01
<b>30 May</b>	85 ± 3	137 ± 1	107 ± 5	21.0 ± 0.8	299 ± 8	54 ± 1	71 ± 2	72 ± 5	10.5 ± 0.4	< SB	29 ± 1	0.127 ± 0.007	4.8 ± 0.2	0.34 ± 0.01
<b>31 May</b>	210 ± 10	311 ± 6	250 ± 10	42 ± 2	375 ± 1	103 ± 5	75 ± 2	170 ± 3	36 ± 1	106 ± 1	136 ± 5	0.163 ± 0.008	6.5 ± 0.3	0.54 ± 0.02
<b>14 June</b>	690 ± 10	680 ± 5	770 ± 30	20.9 ± 0.8	800 ± 10	320 ± 10	131 ± 4	423 ± 2	67 ± 2	136 ± 1	123 ± 5	1.29 ± 0.06	34 ± 1	1.80 ± 0.06
<b>15 June</b>	401 ± 2	470 ± 10	540 ± 20	20.9 ± 0.7	540 ± 10	210 ± 5	102 ± 3	251 ± 2	61 ± 2	133 ± 2	154 ± 6	2.01 ± 0.09	55 ± 2	1.82 ± 0.06
<b>16 June</b>	195 ± 1	243 ± 20	290 ± 10	20.9 ± 0.6	294 ± 4	133 ± 1	97 ± 4	125 ± 1	35 ± 1	80 ± 2	108 ± 5	1.78 ± 0.08	54 ± 2	0.67 ± 0.03
<b>17 June</b>	520 ± 20	610 ± 10	700 ± 30	< 19	660 ± 20	258 ± 1	110 ± 5	353 ± 9	65 ± 2	146 ± 1	141 ± 6	1.75 ± 0.09	52 ± 2	1.15 ± 0.06
<b>18 June</b>	680 ± 20	780 ± 30	740 ± 30	20.9 ± 0.8	870 ± 20	310 ± 10	138 ± 5	454 ± 3	65 ± 3	168 ± 7	132 ± 6	1.76 ± 0.05	51 ± 2	1.56 ± 0.06
<b>19 June</b>	610 ± 60	818 ± 9	850 ± 20	20.9 ± 0.9	780 ± 20	310 ± 30	165 ± 6	370 ± 10	63 ± 2	157 ± 7	100 ± 4	1.53 ± 0.07	46 ± 2	1.37 ± 0.05
<b>20 June</b>	234 ± 6	420 ± 20	490 ± 20	21.1 ± 0.8	469 ± 1	214 ± 1	198 ± 5	167 ± 9	42 ± 1	138 ± 1	116 ± 4	1.46 ± 0.06	41 ± 1	2.11 ± 0.08
<b>02 July</b>	430 ± 20	478 ± 9	550 ± 20	< 19	490 ± 9	218 ± 9	90 ± 4	269 ± 6	42 ± 1	100 ± 4	69 ± 2	0.83 ± 0.02	23 ± 1	0.93 ± 0.04
<b>05 July</b>	570 ± 30	550 ± 20	660 ± 20	< 19	750 ± 20	292 ± 9	126 ± 6	360 ± 10	54 ± 2	122 ± 2	75 ± 3	0.87 ± 0.05	24 ± 1	1.29 ± 0.05
<b>06 July</b>	408 ± 6	490 ± 6	570 ± 20	< 19	530 ± 10	212 ± 3	80 ± 4	276 ± 5	52 ± 2	109 ± 2	67 ± 2	1.32 ± 0.06	36 ± 1	1.16 ± 0.05
<b>07 July</b>	290 ± 10	324 ± 2	310 ± 10	< 19	350 ± 10	161 ± 5	80 ± 3	170 ± 10	27 ± 1	95 ± 6	52 ± 3	1.22 ± 0.05	34 ± 1	0.78 ± 0.03
<b>10 July</b>	235 ± 1	302 ± 1	380 ± 10	< 19	428 ± 1	146 ± 1	100 ± 5	157 ± 2	44 ± 1	30 ± 2	35 ± 2	0.77 ± 0.04	22 ± 1	0.74 ± 0.04
<b>11 July</b>	310 ± 20	280 ± 10	330 ± 20	< 19	390 ± 20	168 ± 10	77 ± 4	180 ± 10	35 ± 1	45 ± 2	31 ± 1	0.88 ± 0.03	28 ± 1	0.84 ± 0.03
<b>14 July</b>	143 ± 4	139 ± 1	175 ± 8	21.0 ± 0.8	199 ± 3	140 ± 10	109 ± 4	74 ± 1	21 ± 1	59 ± 1	59 ± 2	1.13 ± 0.04	27 ± 1	0.43 ± 0.02
<b>15 July</b>	223 ± 4	270 ± 10	316 ± 9	21 ± 1	381 ± 4	160 ± 1	117 ± 4	153 ± 2	36 ± 2	53 ± 5	50 ± 2	0.91 ± 0.03	24 ± 1	0.49 ± 0.03

SB: Sample Blank

**Table 6S.** Minor and trace element (Ba, Cr, Cu, Mn, Ni, Pb, Sn, Ti, V and Zn) concentrations in PM<sub>10</sub> samples. All the results are expressed in ng/m<sup>3</sup>.

	<b>Ba</b>	<b>Cr</b>	<b>Cu</b>	<b>Mn</b>	<b>Ni</b>	<b>Pb</b>	<b>Sn</b>	<b>Ti</b>	<b>V</b>	<b>Zn</b>
<b>25 May</b>	4.36 ± 0.07	< SB	7.5 ± 0.1	5.304 ± 0.007	0.95 ± 0.08	0.76 ± 0.01	2.3 ± 0.2	4.16 ± 0.08	0.27 ± 0.01	8.6 ± 0.3
<b>26 May</b>	4.8 ± 0.1	< SB	10.7 ± 0.5	5.384 ± 0.007	0.87 ± 0.07	0.88 ± 0.03	3 ± 1	3.33 ± 0.09	0.27 ± 0.01	8.6 ± 0.1
<b>27 May</b>	6.1 ± 0.7	0.59 ± 0.09	11.7 ± 0.4	6.3 ± 0.2	2.0 ± 0.4	1.7 ± 0.2	2.9 ± 0.2	7 ± 1	1.7 ± 0.1	14 ± 1
<b>28 May</b>	6.0 ± 0.2	1.23 ± 0.09	9.7 ± 0.9	6.63 ± 0.09	2.62 ± 0.02	2.27 ± 0.06	3.7 ± 0.3	6.7 ± 0.3	2.27 ± 0.03	13 ± 1
<b>29 May</b>	5.6 ± 0.8	0.042 ± 0.002	9.42 ± 0.09	5.63 ± 0.04	1.22 ± 0.02	0.79 ± 0.08	1.5 ± 0.1	4.4 ± 0.7	0.54 ± 0.03	17.0 ± 0.8
<b>30 May</b>	7 ± 1	0.199 ± 0.005	7.3 ± 0.3	5.9 ± 0.3	1.20 ± 0.04	0.54 ± 0.03	2.7 ± 0.3	4.0 ± 0.2	0.23 ± 0.01	22.8 ± 0.3
<b>31 May</b>	8.2 ± 0.3	1.26 ± 0.05	9.4 ± 0.3	8.95 ± 0.04	2.04 ± 0.03	1.22 ± 0.01	3.7 ± 0.1	7.2 ± 0.5	0.66 ± 0.03	18.1 ± 0.3
<b>14 June</b>	14.9 ± 0.1	6.9 ± 0.8	23.0 ± 0.2	30 ± 1	4.9 ± 0.5	7.35 ± 0.07	6.32 ± 0.09	22 ± 1	2.27 ± 0.04	33.7 ± 0.8
<b>15 June</b>	10.4 ± 0.3	1.93 ± 0.02	17.3 ± 0.4	34 ± 2	3.66 ± 0.06	6.1 ± 0.2	6.5 ± 0.3	12.6 ± 0.5	3.8 ± 0.1	23 ± 2
<b>16 June</b>	5.6 ± 0.3	0.089 ± 0.005	10.9 ± 0.2	9.03 ± 0.08	2.85 ± 0.06	2.73 ± 0.08	4.1 ± 0.4	5.4 ± 0.2	4.39 ± 0.05	9.0 ± 0.2
<b>17 June</b>	11.4 ± 0.3	3.25 ± 0.07	19.2 ± 0.3	21.67 ± 0.03	4.4 ± 0.1	4.75 ± 0.05	5.46 ± 0.08	13.0 ± 0.4	3.90 ± 0.07	22.4 ± 0.5
<b>18 June</b>	46.6 ± 0.6	6.0 ± 0.2	21.0 ± 0.7	22.6 ± 0.4	4.8 ± 0.1	4.6 ± 0.1	5.9 ± 0.4	20.6 ± 0.9	3.2 ± 0.1	25.6 ± 0.9
<b>19 June</b>	59 ± 3	5.5 ± 0.7	19.58 ± 0.02	20.9 ± 0.6	3.9 ± 0.2	5.0 ± 0.2	5.0 ± 0.3	20 ± 3	2.5 ± 0.1	49 ± 2
<b>20 June</b>	63 ± 5	3.1 ± 0.1	18.9 ± 0.4	33 ± 7	2.54 ± 0.03	3.2 ± 0.1	4.5 ± 0.2	7.70 ± 0.07	1.94 ± 0.04	43 ± 2
<b>02 July</b>	43.5 ± 0.8	3.6 ± 0.5	14.0 ± 0.5	13.93 ± 0.01	2.9 ± 0.1	3.76 ± 0.06	3.6 ± 0.3	12.9 ± 0.8	1.5 ± 0.1	40 ± 10
<b>05 July</b>	43 ± 1	4.5 ± 0.2	22.1 ± 0.5	21.2 ± 0.7	3.80 ± 0.09	4.4 ± 0.1	5.4 ± 0.2	16 ± 1	1.67 ± 0.08	28.1 ± 0.4
<b>06 July</b>	43 ± 1	3.4 ± 0.1	15 ± 1	20.9 ± 0.1	2.77 ± 0.09	3.5 ± 0.8	4.3 ± 0.6	17 ± 3	1.31 ± 0.07	37 ± 2
<b>07 July</b>	52.0 ± 0.3	1.92 ± 0.07	11 ± 1	19 ± 2	1.8 ± 0.2	3.50 ± 0.03	3.36 ± 0.03	9.6 ± 0.6	0.87 ± 0.01	36.2 ± 0.1
<b>10 July</b>	< SB	4.1 ± 0.1	14.67 ± 0.08	9.9 ± 0.2	2.2 ± 0.2	2.57 ± 0.02	4.10 ± 0.05	8.1 ± 0.2	0.66 ± 0.02	10.8 ± 0.1
<b>11 July</b>	< SB	4.7 ± 0.5	13.1 ± 0.2	11.6 ± 0.6	2.1 ± 0.3	3.0 ± 0.2	3.61 ± 0.08	10 ± 1	0.81 ± 0.05	13.9 ± 0.4
<b>14 July</b>	11.6 ± 0.1	1.48 ± 0.02	8.8 ± 0.2	8.1 ± 0.5	1.47 ± 0.01	2.26 ± 0.02	2.48 ± 0.03	5.5 ± 0.4	1.45 ± 0.01	13.6 ± 0.4
<b>15 July</b>	16.5 ± 0.4	2.54 ± 0.02	15.1 ± 0.8	9.20 ± 0.02	1.9 ± 0.1	2.37 ± 0.05	4.73 ± 0.07	6.8 ± 0.2	1.10 ± 0.01	18.6 ± 0.1

SB: Sample Blank

**Table 7S.** Trace element (As, Cd, Ce, Co, La, Mo, Tl and Zr) concentrations in PM<sub>10</sub> samples. All the results are expressed in pg/m<sup>3</sup>.

	As	Cd	Ce	Co	La	Mo	Tl	Zr
<b>25 May</b>	540 ± 10	34 ± 1	113 ± 8	36 ± 2	87 ± 2	178 ± 7	2.2 ± 0.2	334 ± 17
<b>26 May</b>	600 ± 40	30 ± 4	130 ± 9	25.3 ± 0.7	80 ± 3	217 ± 1	4.0 ± 0.6	340 ± 7
<b>27 May</b>	630 ± 30	35 ± 3	210 ± 20	141 ± 4	140 ± 10	290 ± 20	7.4 ± 0.7	420 ± 50
<b>28 May</b>	625 ± 7	58 ± 1	270 ± 10	168 ± 4	170 ± 10	380 ± 5	7.43 ± 0.03	318 ± 2
<b>29 May</b>	560 ± 20	34 ± 2	92 ± 3	47 ± 2	63.9 ± 0.5	256 ± 5	2.0 ± 0.2	280 ± 10
<b>30 May</b>	593 ± 6	23.6 ± 0.7	80 ± 5	48 ± 6	55 ± 4	450 ± 10	1.78 ± 0.08	510 ± 20
<b>31 May</b>	700 ± 30	129 ± 2	220 ± 10	74 ± 2	124 ± 5	458 ± 3	4.6 ± 0.2	650 ± 30
<b>14 June</b>	1300 ± 100	99 ± 2	770 ± 40	189 ± 8	590 ± 20	1040 ± 10	17.4 ± 0.4	1070 ± 50
<b>15 June</b>	1020 ± 40	90 ± 3	460 ± 10	99 ± 1	388 ± 9	710 ± 20	17.1 ± 0.6	700 ± 10
<b>16 June</b>	780 ± 20	49 ± 2	194 ± 9	50.2 ± 0.2	187 ± 1	485 ± 7	12.0 ± 0.5	380 ± 10
<b>17 June</b>	890 ± 10	69 ± 2	530 ± 20	1060 ± 20	382 ± 9	753 ± 7	16.9 ± 0.2	860 ± 10
<b>18 June</b>	590 ± 10	114 ± 3	618 ± 20	222 ± 3	412 ± 3	930 ± 30	16.3 ± 0.8	1020 ± 40
<b>19 June</b>	569 ± 1	88 ± 3	530 ± 20	210 ± 20	370 ± 10	960 ± 40	24.1 ± 0.9	1000 ± 100
<b>20 June</b>	413 ± 8	82 ± 2	111 ± 1	112 ± 1	119 ± 1	840 ± 20	26.0 ± 0.8	860 ± 10
<b>02 July</b>	345 ± 9	63 ± 3	352 ± 6	130 ± 3	258 ± 3	529 ± 4	10.3 ± 0.3	520 ± 20
<b>05 July</b>	444 ± 6	73 ± 4	450 ± 20	164 ± 5	400 ± 10	910 ± 30	11.7 ± 0.4	820 ± 80
<b>06 July</b>	560 ± 20	91 ± 5	250 ± 10	104 ± 2	320 ± 10	770 ± 50	14.6 ± 0.8	460 ± 40
<b>07 July</b>	490 ± 10	90 ± 2	109 ± 5	63 ± 5	186 ± 3	503 ± 7	15.3 ± 0.3	390 ± 10
<b>10 July</b>	383 ± 4	68 ± 2	85.6 ± 0.2	74 ± 3	85 ± 2	850 ± 20	12.3 ± 0.2	640 ± 10
<b>11 July</b>	390 ± 20	74 ± 4	130 ± 10	97 ± 7	150 ± 10	740 ± 40	14.5 ± 0.9	450 ± 40
<b>14 July</b>	280 ± 4	68 ± 3	< SB	38.6 ± 0.7	165 ± 3	420 ± 6	11.8 ± 0.3	260 ± 4
<b>15 July</b>	353 ± 7	79 ± 3	83 ± 1	95 ± 4	148 ± 4	680 ± 10	10.5 ± 0.2	530 ± 3

SB: Sample Blank

**Table 8S:** Lead isotope ratios (namely  $^{204}\text{Pb}/^{206}\text{Pb}$ ,  $^{206}\text{Pb}/^{207}\text{Pb}$  and  $^{208}\text{Pb}/^{206}\text{Pb}$  ratios) for  $\text{PM}_{10}$  samples collected during start-up phase of the incinerator.

	$^{204}\text{Pb}/^{206}\text{Pb}$	$^{206}\text{Pb}/^{207}\text{Pb}$	$^{208}\text{Pb}/^{206}\text{Pb}$
	Mean $\pm$ SD	Mean $\pm$ SD	Mean $\pm$ SD
<b>25 May</b>	0.0541 $\pm$ 0.0005	1.1532 $\pm$ 0.0003	2.1228 $\pm$ 0.0006
<b>26 May</b>	0.0538 $\pm$ 0.0004	1.1601 $\pm$ 0.0002	2.1186 $\pm$ 0.0004
<b>27 May</b>	0.0526 $\pm$ 0.0004	1.1488 $\pm$ 0.0002	1.8633 $\pm$ 0.0009
<b>28 May</b>	0.0516 $\pm$ 0.0006	1.1597 $\pm$ 0.0009	1.8453 $\pm$ 0.0012
<b>29 May</b>	0.0536 $\pm$ 0.0004	1.1685 $\pm$ 0.0005	2.0825 $\pm$ 0.0012
<b>30 May</b>	0.0532 $\pm$ 0.0001	1.1626 $\pm$ 0.0006	2.0922 $\pm$ 0.0001
<b>31 May</b>	0.0531 $\pm$ 0.0001	1.1635 $\pm$ 0.0006	2.1180 $\pm$ 0.0005
<b>14 June</b>	0.0565 $\pm$ 0.0002	1.1643 $\pm$ 0.0009	2.0561 $\pm$ 0.0018
<b>15 June</b>	0.0551 $\pm$ 0.0006	1.1642 $\pm$ 0.0003	2.0176 $\pm$ 0.0003
<b>16 June</b>	0.0519 $\pm$ 0.0003	1.1677 $\pm$ 0.0005	1.9363 $\pm$ 0.0001
<b>17 June</b>	0.0543 $\pm$ 0.0006	1.1308 $\pm$ 0.0002	2.0266 $\pm$ 0.0008
<b>18 June</b>	0.0557 $\pm$ 0.0002	1.1370 $\pm$ 0.0009	2.0212 $\pm$ 0.0014
<b>19 June</b>	0.0566 $\pm$ 0.0002	1.1686 $\pm$ 0.0001	2.0159 $\pm$ 0.0025
<b>20 June</b>	0.0514 $\pm$ 0.0006	1.1721 $\pm$ 0.0003	1.8929 $\pm$ 0.0041
<b>02 July</b>	0.0522 $\pm$ 0.0004	1.1363 $\pm$ 0.0009	1.9752 $\pm$ 0.0007
<b>05 July</b>	0.0535 $\pm$ 0.0003	1.1344 $\pm$ 0.0011	2.0354 $\pm$ 0.0015
<b>06 July</b>	0.0530 $\pm$ 0.0008	1.1448 $\pm$ 0.0012	1.9576 $\pm$ 0.0043
<b>07 July</b>	0.0501 $\pm$ 0.0004	1.2073 $\pm$ 0.0005	1.8884 $\pm$ 0.0015
<b>10 July</b>	0.0512 $\pm$ 0.0003	1.1883 $\pm$ 0.0007	1.9085 $\pm$ 0.0002
<b>11 July</b>	0.0504 $\pm$ 0.0004	1.1933 $\pm$ 0.0008	1.8789 $\pm$ 0.0039
<b>14 July</b>	0.0505 $\pm$ 0.0003	1.1962 $\pm$ 0.0005	1.9126 $\pm$ 0.0014
<b>15 July</b>	0.0504 $\pm$ 0.0001	1.2118 $\pm$ 0.0009	1.8836 $\pm$ 0.0006